Available online at www.sciencedirect.com
ScienceDirect
Remote Sensing of Environment 109 (2007) 342–360
Remote Sensing of Environment
www.elsevier.com/locate/rse

Mapping tree and shrub leaf area indices in an ombrotrophic peatland through multiple endmember spectral unmixing

O. Sonnentag [a,*], J.M. Chen [a,1], D.A. Roberts [b,2], J. Talbot [c,3], K.Q. Halligan [b,2], A. Govind [a,1]

[a] University of Toronto, Department of Geography and Planning, St. George Campus, Sidney Smith Hall, 100 St. George St., Room 5047, Toronto, ON, Canada M5S 3G3
[b] University of California Santa Barbara, Department of Geography, 3611 Ellison Hall, Santa Barbara, CA, 93106-4060, USA
[c] McGill University, Department of Geography, Burnside Hall, 805 Sherbrooke West, Room 705, Montreal, QC, Canada H3A 2K6

Received 12 October 2006; received in revised form 8 January 2007; accepted 13 January 2007

Abstract

Leaf area index (LAI) is an important parameter used by most process-oriented ecosystem models. LAI of forest ecosystems has routinely been mapped using spectral vegetation indices (SVI) derived from remote sensing imagery. The application of SVI-based approaches to map LAI in peatlands presents a challenge, mainly due to peatlands characteristic multi-layer canopy comprising shrubs and open, discontinuous tree canopies underlain by a continuous ground cover of different moss species, which reduces the greenness contrast between the canopy and the background.

Our goal is to develop a methodology to map tree and shrub LAI in peatlands and similar ecosystems based on multiple endmember spectral mixture analysis (MESMA). This new mapping method is validated using LAI field measurements from a precipitation-fed (ombrotrophic) peatland near Ottawa, Ontario, Canada. We demonstrate first that three commonly applied SVI are not suitable for tree and shrub LAI mapping in ombrotrophic peatlands. Secondly, we demonstrate for a three-endmember model the limitations of traditional linear spectral mixture analysis (SMA) due to the unique and widely varying spectral characteristics of *Sphagnum* mosses, which are significantly different from vascular plants. Next, by using a geometric-optical radiative transfer model, we determine the nature of the equation describing the empirical relationship between shadow fraction and tree LAI using nonlinear ordinary least square (OLS) regression. We then apply this equation to describe the empirical relationships between shadow and shrub fractions obtained from mixture decomposition with SMA and MESMA, respectively, and tree and shrub LAI, respectively. Less accurate fractions obtained from SMA result in weaker relationships between shadow fraction and tree LAI ($R^2=0.61$) and shrub fraction and shrub LAI ($R^2=0.49$) compared to the same relationships based on fractions obtained from MESMA with $R^2=0.75$ and $R^2=0.68$, respectively. Cross-validation of tree LAI ($R^2=0.74$; RMSE=0.48) and shrub LAI ($R^2=0.68$; RMSE=0.42) maps using fractions from MESMA shows the suitability of this approach for mapping tree and shrub LAI in ombrotrophic peatlands. The ability to account for a spectrally varying, unique *Sphagnum* moss ground cover during mixture decomposition and a two layer canopy is particularly important.

Keywords: Leaf area index; LAI-2000; Peatlands; Spectral mixture analysis; SMA; MESMA

1. Introduction

Peatlands, which are wetlands that accumulate partially decayed plant matter as peat, are an extensive component of boreal and subarctic ecozones. In Canada, they cover about 14% of the land area (Tarnocai et al., 2000). Bogs are common types of peatlands which are precipitation-fed (ombrotrophic) and generally lack any other hydrological inputs, resulting in acidic and nutrient-poor conditions. The characteristic multi-layer canopy of bogs comprises a *Sphagnum* moss ground cover under ericaceous shrubs, and patches of sparse coniferous trees. Due to this vertical vegetation structure, a substantial proportion of the solar energy reaches the shrub canopy resulting in a significant role for shrubs in carbon, water, and energy exchanges with the atmosphere (e.g., Baldocchi et al., 2000; Lafleur et al., 2005; Moore et al., 2002).

* Corresponding author. Tel.: +1 416 946 7715; fax: +1 416 946 3886.
E-mail address: oliver.sonnentag@utoronto.ca (O. Sonnentag).
[1] Tel.: +1 416 946 7715; fax: +1 416 946 3886.
[2] Tel.: +1 805 893 2276.
[3] Tel.: +1 514 398 4111.

0034-4257/$ - see front matter © 2007 Elsevier Inc. All rights reserved.
doi:10.1016/j.rse.2007.01.010

Peat accumulation is the result of net primary productivity (NPP), the net gain of carbon in the form of biomass through photosynthesis, persistently exceeding the decomposition of organic matter. Peatlands act as long term stores of carbon with an average long-term apparent carbon accumulation rate of 15–30 g C m^{-2} $year^{-1}$ (Turunen et al., 2002). As a result, peatlands store up to 450 Gt C or one third of the global soil carbon (Gorham, 1991; Turunen et al., 2002). The role of peatlands as long-term carbon sinks in the global carbon cycle is closely related to climatic conditions. Possible responses of peatlands to climatic changes might include shifts in peatland distribution and extent, and a switch from long-term sinks to long-term sources of atmospheric carbon (e.g., Gorham, 1991; Moore et al., 1998).

A promising means to quantify possible responses of peatland carbon dynamics to likely climatic changes is the use of process-oriented ecosystem models as predictive tools. An important parameter of most process-oriented ecosystem models is the leaf area index (LAI). LAI is a dimensionless quantity of the amount of foliage area of a vegetation canopy and is defined as one half the total leaf area (all-sided) per unit ground horizontal surface area (Chen & Black, 1992). LAI characterizes the canopy–atmosphere interface of an ecosystem, and is therefore related to precipitation and atmospheric nutrient deposition interception, canopy microclimate, radiation extinction, and water, carbon, and energy exchanges with the atmosphere. Some process-oriented models such as the Boreal Ecosystem Productivity Simulator (BEPS; Liu et al., 1997) use LAI as an input parameter, while others such as the Peatland Carbon Simulator (PCARS; Frolking et al., 2002) generate LAI as a function of foliar biomass. For the parameterization of distributed, process-oriented ecosystem models such as BEPS, tree LAI in forest ecosystems has traditionally been mapped based on ordinary least square (OLS) regression analysis relationships between field-measured tree LAI and various spectral vegetation indices (SVI) derived from remote sensing imagery. Common SVI used for this purpose are the normalized difference vegetation index (NDVI; Deering, 1978), [(NIR − red)/(NIR + red)], the simple ratio (SR; Jordan, 1969), [NIR/red], and the reduced simple ratio (RSR; Brown et al., 2000), $[SR * (1 - (SWIR - SWIR_{min})/(SWIR_{max} - SWIR_{min}))]$ (Chen & Cihlar, 1996; Chen et al., 2002; Eklundh et al., 2003). However, the multi-layer canopy of ombrotrophic peatlands limits the applicability of SVI-based approaches to map tree LAI due to the discontinuity and openness of the tree canopy consisting of spatially distinct crowns resulting in increased shadow fraction, and due to the reduced greenness contrast between the canopy and the background.

Background reflectance in ombrotrophic peatlands varies depending on the vertical vegetation structure within the peatland. In forested portions, sunlit trees are the principal contributor to the overall spectral response. The background reflectance, mainly determined by crown closure, is composed of the spectral reflectance of tree and shrub shadow on neighbouring trees, shrubs, and mosses, sunlit shrubs and mosses, and, in places, open water. In open portions where trees are absent, sunlit shrubs are the principal contributors to the overall spectral response. Here, the background reflectance, mainly determined by shrub canopy closure, is composed of shrub shadow on neighbouring shrubs and mosses, sunlit mosses, and, in places, open water. Thus, in both forested and open portions, the background reflectance contributing to the overall spectral response is partially controlled by the spectral characteristics of mosses, which are significantly different from vascular plants in the visible, NIR, and short-wave infrared (SWIR) ranges of the electromagnetic spectrum (Bubier et al., 1997).

Alternative approaches to map tree LAI in forest ecosystems based on remote sensing imagery include the application of inverse OLS and reduced major axis (RMA) regression analysis, and geostatistical techniques such as cokriging, kriging with external drift (KED), and sequential Gaussian conditional simulation (SGCS) (Berterretche et al., 2005; Cohen et al., 2003). Another promising route to map tree LAI in forest ecosystems was proposed by Hall et al. (1995). In their study they demonstrated empirically and theoretically that the scene fractions of shadow and sunlit background obtained by mixture decomposition of a three-endmember model (sunlit tree canopy, sunlit background, and shadow) with linear spectral mixture analysis (SMA) were related to biophysical parameters such as LAI. The dependence of these fractions on solar zenith angle < 50° (SZA) was shown to be minimal. SMA-based approaches to map tree LAI were also pursued by Hall et al. (2003), Hu et al. (2004), and Peddle et al. (1999).

Considering the importance of the shrub canopy in the overall hydrological and ecological functioning of peatlands, its reliable parameterization in distributed, process-oriented ecosystem models in addition to the tree canopy is mandatory. However, none of the existing remote sensing-based methods allows for the separate mapping of tree and shrub LAI of a multi-layer canopy comprising shrubs and open, discontinuous tree canopies. Our goal was to develop a methodology for tree and shrub LAI mapping in ombrotrophic peatlands and similar ecosystems based on field measurements, geometric-optical radiative transfer modelling, and multiple endmember spectral mixture analysis (MESMA; Roberts et al., 1998). MESMA is an extension of SMA that takes into account the spectral variability within endmembers and optionally allows the number of endmembers to vary on a per-pixel basis. To achieve our goal we carefully quantified tree and shrub LAI during peak growing season in the Mer Bleue bog using the LAI-2000 plant canopy analyzer. This included the determination of previously unavailable species-specific LAI-2000 correction factors for tamarack. The multi-layer canopy of the bog and its species composition are typical for ombrotrophic peatlands (Payette & Rochefort, 2001). Furthermore, we tested the applicability of NDVI, SR, and RSR for tree and shrub LAI mapping, and demonstrated the superiority of MESMA over SMA in ombrotrophic peatlands due to the unique and widely varying spectral characteristics of *Sphagnum* mosses.

2. Materials and methods

2.1. Site description and transect locations

The Mer Bleue bog (45.4°N latitude, 75.5°W longitude) is a raised, ombrotrophic peatland, about 10 km south-east of

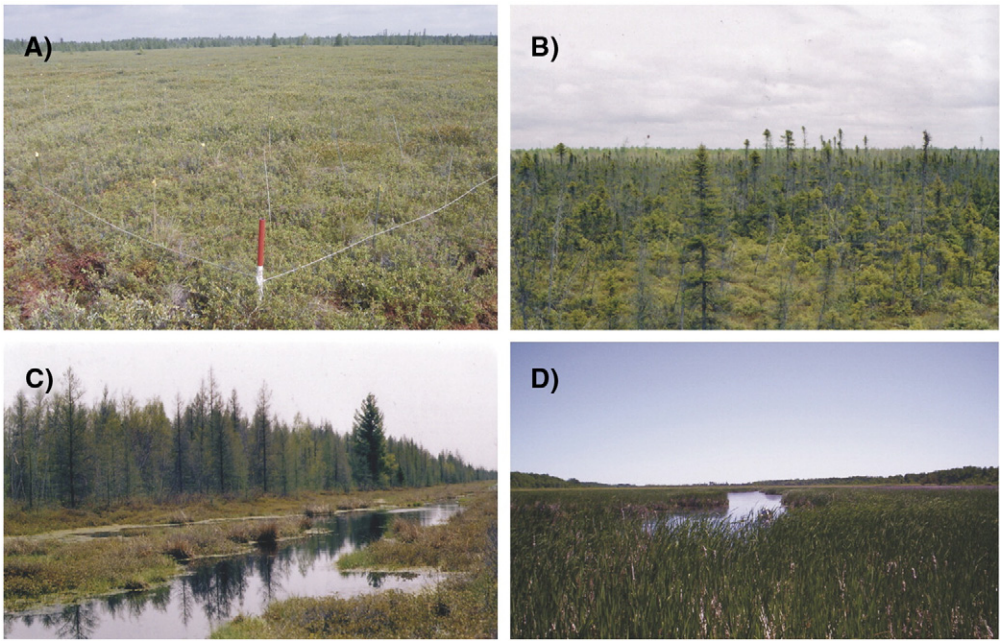

Fig. 1. Dominant species composition and vegetation structures occurring at Mer Bleue: A) pristine shrub canopy comprising evergreen and deciduous shrubs, B) sparse patches of pristine tree canopy comprising mainly tamarack and black spruce, C) relatively dense mixed tree canopy along a drainage ditch, and D) mineral wetland (marsh) comprising mainly cattail (the approximate locations of all photographs are given in Fig. 2).

Ottawa, Ontario, Canada. It covers an area of about 28 km^2 and is roughly oval shaped with an east–west orientation. The climate of the region is cool continental, with a 30-year (1971–2000) mean annual temperature of 6.0±0.8 °C. Sub-surface water and sometimes surface water is shed from the gently domed central part of the bog towards its margins, where it drains away along beaver ponds surrounding the bog (Roulet et al., 2006). The pristine (undisturbed) species composition of Mer Bleue bog is characterized by dominant evergreen shrubs (*Chamaedaphne calyculata*, *Ledum groenlandicum*, *Kalmia ngustifolia*, *Kalmia polifolia*, *Andromeda glaucophylla*), deciduous shrubs (*Vaccinium myrtilloides*) (Fig. 1A), and sparse patches of sedges (*Eriophorum spissum*), black spruce (*Picea mariana*) and tamarack (*Larix laricina*) trees, and occasional grey birch (*Betula populifolia*) and white birch (*Betula papyrifera*) trees (Fig. 1B). The average canopy height is about 0.20 m and 3 m for the shrub and sparse tree canopy, respectively. The surface of the bog is covered by species of *Sphagnum* moss (*Sp. angustifolium*, *Sp. capillifolium*, *Sp. magellanicum*, and *Sp. fuscum*). Characteristic features of the bog are distinct microforms consisting of hollows, hummocks, and intermediate lawns, with a mean relief between hollows and hummocks of 0.25 m (Lafleur et al., 2005).

The species composition along narrow bands of several approximately north–south oriented drainage ditches is characterized by a relatively dense mixed tree canopy that consists primarily of tamarack and grey birch with interspersed black spruce and white pine (*Pinus strobus*) (Fig. 1C). The average tree canopy height is about 10 m. The species composition of the shrub canopy in these areas is the same as for the rest of the bog, but reaches an average height of 1 m. The patchy ground cover is composed of *Sphagnum* and brown mosses. This vertical vegetation structure reflects the drained conditions along drainage ditches and in the transition between the peat body and surrounding mineral wetlands (cattail marsh). The cattail marshes are dominated by narrow-leaved cattail (*Typha angustifolia*) with an average height of about 2.5 m (Fig. 1D). In the following we use "Mer Bleue bog" to refer to the ombrotrophic peatland characterized by pristine species composition and vertical vegetation structure, whereas "Mer Bleue" is used to refer to the ombrotrophic peatland and the surrounding mineral wetlands as defined by the National Capital Commission (Ottawa, Ontario, Canada) (Fig. 2).

Using the LAI-2000 plant canopy analyzer (Norman & Welles, 1991; Li-COR, Lincoln, Nebraska, USA), we measured tree LAI along five transects (mbt1, mbt2, mbt3, mbt4, and mbt5) and shrub LAI along eight transects (mbt1, mbt2,

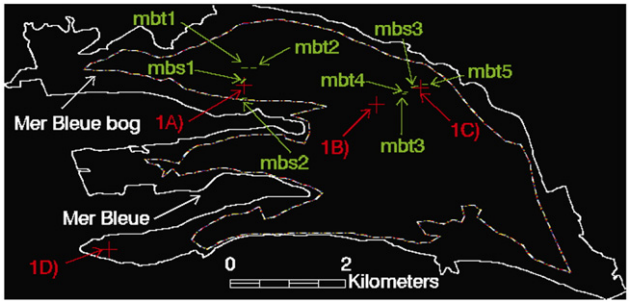

Fig. 2. Transect (green) and approximate photograph (red) locations of Fig. 1 within Mer Bleue (after National Capitol Commission, Ottawa, Ontario, Canada) and Mer Bleue bog (approximate boundary).

Table 1
Transect characteristics (d=disturbed)

Transect	Length [m]	Orientation	Species composition
mbt1	100	E–W	Tamarack/mixed shrubs
mbt2	100	E–W	Black spruce/mixed shrubs
mbt3	50	~E–W	Tamarack/black spruce/mixed shrubs
mbt4	50	~E–W	Tamarack/black spruce/mixed shrubs
mbt5	100	E–W	Mixed forest/mixed shrubs (d)
mbs1	100	NE–SW	Mixed shrubs
mbs2	100	NE–SW	Mixed shrubs
mbs3	100	NE–SW	Mixed shrubs

mbt3, mbt4, mbt5, mbs1, mbs2, and mbs3) in August 2005 (Fig. 2).

All transects were 50 m or 100 m in length, and oriented in northeast–southwest or east–west direction (Table 1). Along each transect a forestry flag was placed every 10 m to serve as a distance marker. The positions of all flags were recorded in UTM coordinates (North American Datum 1983) using a GPSMAP76 global positioning system (Garmin International Inc., Olathe, KS, USA).

For the tree transects, basal area and stand density (just for mbt3, mbt4, and mbt5), and for the shrub transects, species composition and percent cover, were estimated at each flag position (within a 50×50 cm plot with the flag in the center) prior to the LAI-2000 measurements.

2.2. LAI field and laboratory measurements

The LAI-2000 instrument measures canopy gap fractions by detecting blue diffuse light (between 400 and 490 nm) penetrating the canopy with quantum detectors arranged in five concentric rings. The LAI estimate obtained from the LAI-2000 instrument is an "effective" LAI (LAI_e) derived from the light interception of all canopy elements using a radiative transfer model (Chen, 1996; Chen et al., 1997).

All LAI-2000 measurements were taken at dusk or dawn, i.e. under diffuse sky conditions, to minimize the effect of multiple scattering of light within the canopies and to prevent direct sunlight on the instrument sensor. To avoid any effects of the operator on the instrument sensor, a 270° view cap was used for all measurements. The post-processing of all measurements was accomplished using the LAI-2000 analysis software provided by LI-COR (F2000.exe). As part of the post-processing, the outer two rings of the quantum sensor were excluded from the final calculation of LAI_e to (i) decrease the influence of stronger multiple light scattering effects at larger zenith angles (Chen et al., 2006; Sonnentag et al., in press), to (ii) eliminate the additional effect of the microtopographic position of the LAI-2000 measurement for shrub LAI (Sonnentag et al., in press), and to (iii) minimize the potential field of view of the quantum sensor to roughly 0.9 times the average canopy height (with the inner three rings the sensor's view limit is 43° and tangent (43°) is 0.9) to guarantee measurement independence along the transects.

Based on theoretical considerations and subsequent validation, Chen (1996) and Chen et al. (1997) introduced the following equation to derive tree LAI of boreal forest canopies from LAI_e:

$$LAI = (1-\alpha)LAI_e \frac{\gamma_E}{\Omega_E} \quad (1)$$

where α is the woody-to-total leaf area ratio (to account for the contribution of woody canopy elements to light interception), LAI_e is the "effective" LAI [m^2/m^2], γ_E is the needle-to-shoot area ratio (to account for clumping within shoots), and Ω_E is the element clumping index (to account for clumping at spatial scales larger than shoots). Tree LAI for each flag of the tree transects was calculated from LAI_e using Eq. (1). A critical component in the application of Eq. (1) is the reliable estimation of γ_E, Ω_E, and especially α (Chen et al., 2006).

For the estimation of γ_E for tamarack, we followed the approach of Chen (1996). Since *Larix* sp. are a shade intolerant species (Olaczek, 1986), we took shoot samples from tamarack trees growing under two different growth conditions in terms of light availability. A total of 45 shoot samples were taken from trees of a central forest patch (referred to as forested bog): one dominant (D), one co-dominant (M), and one suppressed (S) tree, at three different height levels: top (T), middle (M), and bottom (L), resulting in nine classes with five shoot samples each: DT, DM, DL, MT, MM, ML, MS, ST, SM, and SL. To guarantee sampling consistency, the same sampling scheme according to tree height was applied to randomly selected, isolated trees (with one tree corresponding to the average height of each dominance category) located in an open area of the Mer Bleue bog (referred to as open bog), also resulting in a total of 45 shoot samples. All 90 shoot samples were stored in electrical coolers at a temperature of around 0° and analyzed in the laboratory within 3 days of sampling. Projected shoot areas for the simplified 3-angle projection method of Chen (1996) were measured using the apparatus described by Chen et al. (2006). The apparatus consists of a Toshiba PDR-4300 digital camera (Toshiba American Information Systems Inc., Irvine, CA, USA) mounted on a firm stand, a Prolite 5000 light box (Kaiser Fototechnik GmbH & Co. KG, Buchen, Baden-Wuerttemberg, Germany), and the WinSeedle (v2003a) image analysis software (Regent Instruments Inc., Quebec City, Quebec, Canada). A volume displacement method was used to measure the total needle area in a shoot (Chen et al., 1997). The conversion of the displaced volume to the surface area of tamarack needles was accomplished with an empirical equation for needles with elliptical cross sections according to the needle thickness-to-width ratio provided by Chen et al. (2006). For black spruce we used $\gamma_E = 1.36$ as estimated by Chen (1996).

For the quantification of clumping at spatial scales larger than shoots we used the Tracing Radiation and Architecture of Canopies (TRAC) instrument (3rd Wave Engineering, Napean, Ontario, Canada) based on a gap size distribution theory (Chen & Cihlar, 1995) to measure Ω_E directly in the field. The TRAC instrument was used five times each along mbt1 and mbt2 on sunny days during the last week of August 2005 to determine Ω_E for black spruce and tamarack separately.

The biggest source of uncertainty in the application of Eq. (1) is considered to be α. Ideally, its reliable estimation

requires destructive sampling (Chen et al., 2006). For black spruce we used $\alpha = 0.15$ as provided by Chen et al. (2006). Due to the logistical constraints of harvesting a tree, we approximated α for tamarack by taking the average of two estimates of α determined with two different methods. The first estimate of α was based on a set of tree morphological measurements in combination with intermediate results obtained from the estimation of γ_E for tamarack (Appendix A). The second estimate of α was based on seven growing and non-growing season (leaf-off) LAI-2000 measurements (Barr et al., 2004), taken at the same seven flags of mbt1.

Finally, tree LAI for each flag was calculated from LAI_e using Eq. (1) with γ_E, Ω_E, and α weighted according to basal area (data not shown) for black spruce and tamarack.

Shrub LAI for each flag of the tree and shrub transects was calculated from LAI_e with a simplified version of Eq. (1) following Sonnentag et al. (in press):

$$LAI = (1-\alpha)LAI_e \quad (2)$$

where α is the woody-to-total area ratio, weighted according to percent cover of each species at each flag (data not shown). Species-specific values for α for the shrub canopy of Mer Bleue bog are provided by Sonnentag et al. (in press).

2.3. Multiple endmember spectral mixture analysis

Mixture decomposition with SMA is a widely applied technique in passive optical remote sensing for determining fractions of pixel components. SMA has been successfully applied in a wide range of disciplines including forestry (e.g., Roberts et al., 2004), geology (e.g., Bryant, 1996), social sciences (e.g., Schweik & Green, 1999), and urban studies (e.g., Wu & Murray, 2003). In SMA it is assumed that the spectral reflectance of a pixel (ρ'_λ) is a mixture of the spectral reflectance of individual scene components (endmembers), each weighted according to their abundance to produce the mixture. Furthermore, it is typically assumed that the mixture is linear and that multiple scattering is negligible resulting in minimal interaction between scene elements (Adams et al., 1993; Hall et al., 1995; Roberts et al., 1993). The model is described by:

$$\rho_\lambda{}' = \sum_{i=1}^{N} f_i * \rho_{i\lambda} + \varepsilon_\lambda \quad (3)$$

where $\rho_{i\lambda}$ is the spectral reflectance of endmember i for a specific band (λ), f_i is the fraction of the endmember, N is the number of endmembers, and ε_λ is the residual error. A common way to assess the fit of an endmember model is by the root mean square error (RMSE), calculated as:

$$RMSE = \sqrt{\frac{\sum_{\lambda=1}^{M} (\varepsilon_\lambda)^2}{M}} \quad (4)$$

where M is the number of bands. To produce accurate fractions, two constraints have to be imposed on the mixture decomposition. The first constraint requires that the fractions sum up to one and the second constraint requires the fractions to be non-negative (Heinz & Chang, 2001).

One of the most critical steps in the application of mixture decomposition is the selection and proper spectral characterization of suitable endmembers (Dennison & Roberts, 2003a; Tompkins et al., 1997). The spectral signature of endmembers can be determined by spectroradiometer measurements in the field or in the laboratory, selection of "pure" endmember pixels from the image to be unmixed, or simulation with a radiative transfer model. However, using a fixed set of endmembers, each with a single invariant spectral signature is a significant simplification of the real world and a fundamental limitation of SMA since it might result in poor accuracy of fractions (Petrou & Foschi, 1999; Song, 2005; Theseira et al., 2003). Furthermore, SMA uses the same number of endmembers for each pixel, not considering whether the respective endmember is present in a pixel or not. To overcome these two limitations of SMA, Roberts et al. (1998) introduced multiple endmember spectral mixture analysis (MESMA) to account for the spectral variability of endmembers and the varying number of endmembers on a per-pixel basis. In MESMA, endmembers for mixture decomposition are selected from a site-specific spectral library containing the spectral signatures of suitable endmembers. The endmember combination producing the lowest RMSE is assigned to each pixel (Roberts et al., 1998).

MESMA has been successfully applied in a wide range of remote sensing studies including snow cover and area mapping (e.g., Painter et al., 2003), plant species mapping (e.g., Dennison & Roberts, 2003a,b; Roberts et al., 1998, 2003), soil mapping in arid lands (e.g., Okin et al., 2001), landform mapping (e.g., Ballantine et al., 2005), fire temperature mapping (e.g., Dennison et al., 2006), urban morphology (e.g., Rashed et al., 2003), and planetary mapping (e.g., Johnson et al., 2006; Li & Mustard, 2003).

Based on field observations, the spectral similarity among tree and shrub canopies found in an exploratory study (data not shown), and aerial photographs, it was determined that a three endmember model consisting of a general sunlit vascular plant canopy, sunlit *Sphagnum* moss, and shadow would be

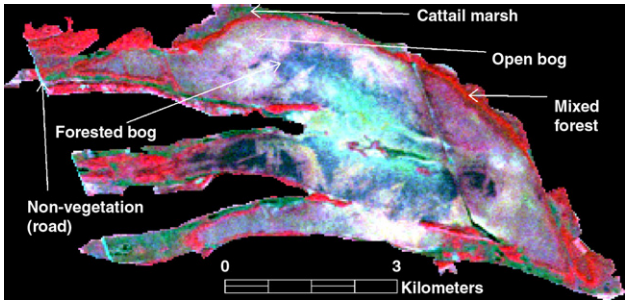

Fig. 3. False color composite (4, 3, 2 band combination) of the clipped subset of the Landsat TM scene of Mer Bleue, demonstrating the different spectral characteristics of the five considered land cover classes.

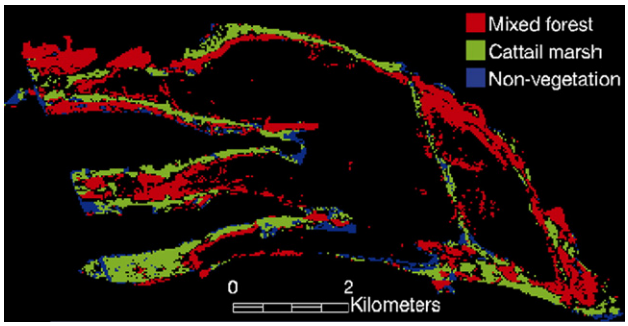

Fig. 4. Mixed forest, cattail marsh, and non-vegetation pixels excluded from the Mer Bleue subset with SAM to obtain the open and forested portions of Mer Bleue bog with pristine species composition and vertical vegetation structure for spectral unmixing.

suitable for Mer Bleue bog. The spectral characterization of the sunlit *Sphagnum* moss and shadow endmembers was accomplished with branch scale spectroradiometer measurements in the field (Section 2.4). The sunlit vascular plant canopy endmember was spectrally characterized using "pure" image pixels (Section 2.5). For both SMA and MESMA, fractions were constrained to sum to 1 and RMSE was restricted to ≤ 0.025. Pixels exceeding this RMSE value were left unmodelled. No negative or superpositive abundance fractions were allowed for the sunlit vascular plant canopy ang sunlit *Sphagnum* moss endmembers. No minimum abundance fraction for the shadow endmember was set. Its maximum abundance fraction was set to 0.80.

Mixture decomposition with SMA and MESMA on Landsat TM bands 1 through 5 was performed with VIPER Tools developed at the Department of Geography at University of California Santa Barbara as an add-on for the ENVI software package (http://www.vipertools.org).

2.4. Spectral measurements

We measured the spectral reflectance of "pure" *Sphagnum* moss ground cover (for the spectral characterization of the sunlit *Sphagnum* moss endmember), the shrub canopy with a *Sphagnum* moss ground cover background (for the parameterization of the geometric-optical radiative transfer model in Section 2.6), and tree and shrub shadows at the branch scale (for the spectral characterization of the shadow endmember) between 350 and 2500 nm at 2 nm sampling intervals in the field with a FieldSpec Pro spectroradiometer (Analytical Spectral Devices (ASD) Inc., Boulder, Colorado, USA) during the last week of August 2005. To capture the intra-canopy variability in spectral reflectance of shrubs and the inter-species as well as the intra-species variability in spectral reflectance of *Sphagnum* moss as influenced by different volumetric moss moisture contents and environmental conditions, we took several sets of spectral reflectance measurements at different locations with

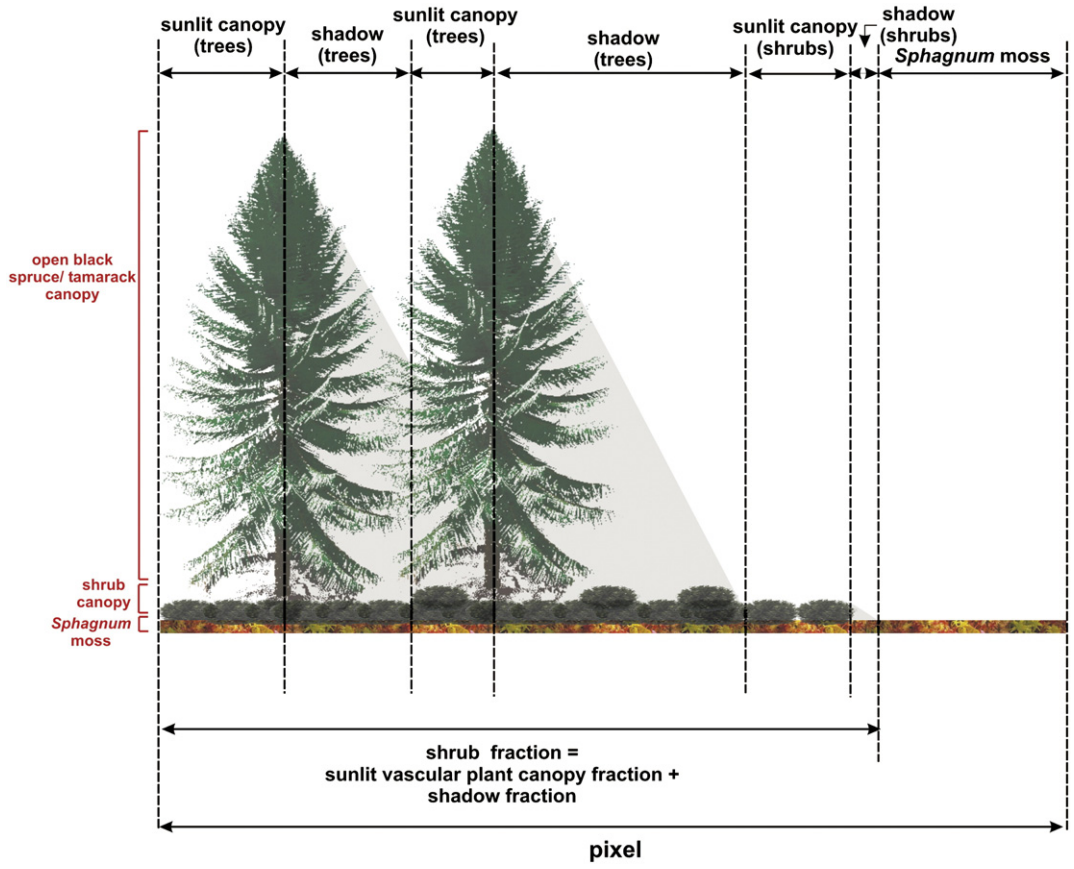

Fig. 5. Conceptualization of our shrub LAI mapping approach: the open tree canopy and its shadow are both "underlain" by shrub canopy, and thus the shrub fraction of a pixel is the sum of the sunlit vascular plant canopy and shadow fractions, i.e. [1 − sunlit *Sphagnum* moss fraction].

different shrub and *Sphagnum* moss species under different moisture conditions across the bog. Each set of spectral reflectance measurements consisted of six individual measurements taken within a radius of 0.5 m. All spectral reflectance measurements were taken between 10 am and 2 pm at a height of about 0.25–0.30 m above the target (sensor field of view: 25°), and were standardized to reflectance using a Spectralon diffuse reflectance target (Labsphere, North Sutton, New Hampshire, USA). The raw data of all spectral measurements acquired for this study are available from the corresponding author upon request.

2.5. Landsat TM image preprocessing

The Landsat TM scene at 30 m-resolution used in this study was acquired September 6, 2005. The scene was ordered as a radiometrically and geometrically corrected L1G product in UTM coordinates (North American Datum 1983). The digital numbers of the scene were transformed into radiance values at the top of the atmosphere by using the gains and offsets provided with the image. The atmospheric correction to convert the radiance values at the top of the atmosphere into spectral reflectance values at the ground surface was accomplished with the Second Simulation of Satellite Signal in the Solar Spectrum (6S) code (Vermote et al., 1997) using atmospheric conditions from Ottawa at the date of scene acquisition as input. The atmospheric water vapour and ozone burden data required by 6S were obtained from the Moderate Resolution Imaging Spectroradiometer (MODIS) Atmospheric Profile data product (http://daac.gsfc.nasa.gov/MODIS/). Atmospheric optical depth which is crucial in the derivation of spectral reflectance values at the ground surface from radiance values at the top of the atmosphere was simulated by 6S based on a standard continental aerosol profile using the meteorological parameter "visibility" as provided for Ottawa for the date of scene acquisition by Environment Canada (http://climate.weatheroffice.ec.gc.ca). All subsequent processing steps related to the calculation of SVI, SMA, and MESMA were performed on a subset of the Landsat TM scene, clipped to the boundary of Mer Bleue (Fig. 3). For our purposes of peatland LAI mapping we distinguish between the five land cover classes "open bog", "forested bog", "mixed forest", "cattail marsh", and "non-vegetation" (including open water and roads), all of which have significantly different spectral characteristics (Fig. 3).

To test the applicability of common SVI for peatland LAI mapping, we computed NDVI, SR, and RSR for OLS regression analysis with our tree and shrub LAI field measurements.

Our LAI mapping efforts with MESMA were aimed at the open and forested portions of Mer Bleue bog with pristine species composition and vertical vegetation structure (Fig. 3). Therefore, parts of Mer Bleue that are characterized by mixed forest, cattail marsh or non-vegetation were identified and excluded prior to mixture decomposition using the Spectral Angle Mapper (SAM; Kruse et al., 1993), a supervised classification method (Fig. 4). The spectral characterization of the reference reflectance spectra for SAM and the sunlit vascular plant canopy endmember of our three-endmember model was accomplished with the Minimum Noise Feature (MNF) transformation (Green et al., 1988) and the Pixel Purity Index (PPI; Boardman et al., 1995) applied to MNF transformed data for the identification of spectrally "pure" pixels as implemented in the ENVI software package (ENVI, 2004). To guarantee that we obtain just the purest pixels for mixed forest, cattail marsh, non-vegetation, and the sunlit vascular plant canopy endmember, we applied the PPI approach successively, using different PPI thresholds for the four different classes. For SAM and spectral endmember characterization we averaged the 10 purest pixels of each class.

2.6. Tree and shrub LAI mapping

Inspired by the study of Hall et al. (1995), which empirically and theoretically demonstrates the relationship between shadow fraction and tree LAI, we investigated the nature of this relationship for the Mer Bleue bog using the geometric-optical radiative transfer model 4-Scale (Chen & Leblanc, 1997) and nonlinear OLS regression analysis. Our hyperspectral 4-Scale simulations were aimed to calculate shadow fractions for tree LAI values ranging from 0 to 3 for a spatial domain of the size of a Landsat TM pixel (900 m^2). The calculation of domain fractions with 4-Scale requires information on the optical properties of foliage and background in the form of hyperspectral leaf scale transmittance and reflectance spectra and hyperspectral branch scale reflectance spectra, respectively. To investigate the nature of the regression relationship between tree LAI and shadow fraction, we used the sum of shaded crown and shaded background as the total shadow fraction of our modelling domain. Details on the major features of 4-Scale and information on its parameterization for this study is provided in Appendix B.

All tree and shrub transects were located on the Landsat TM scene. To estimate the average tree and shrub LAI for Landsat TM pixels along transects, all LAI-2000 field measurements taken within each transect pixel were averaged. In total, we obtained 17 pixels of the forested portions of Mer Bleue bog to which we were able to assign an average value of field-measured tree LAI (LAI-2000 instrument). Depending on the relative location of each transect on the Landsat TM scene, the number of field-measured tree LAI per pixel varied between one (for three pixels) and four (for one pixel), respectively. Average tree LAI of six and seven pixels was based on two and three field measurements, respectively.

Tree LAI of the forested portions of Mer Bleue bog was mapped through inversion of the equation describing the empirical relationship between shadow fraction obtained from mixture decomposition and tree LAI as determined through our simulations with 4-Scale. Tree LAI for the mixed forest pixels of Mer Bleue (Fig. 4) was mapped through inversion of the published exponential equation of the empirical relationship between RSR and mixed forest tree LAI provided by Chen et al. (2002):

$$\mathrm{RSR} = 9.3 - 9.3e^{(-\mathrm{LAI}/2.93)}. \quad (5)$$

Regarding shrub LAI, we obtained 29 pixels in total, 15 pixels corresponding to tree transects (two of the 17 pixels of

the forested portions close to a drainage ditch were neglected because the shrub canopy reached an average height of 1 m) and 14 pixels corresponding to shrub transects, to which we were able to assign an average value of field-measured shrub LAI (LAI-2000 instrument). The number of field-measured shrub LAI per pixel varied between one (for five pixels) and four (for two pixels), respectively. Average shrub LAI of 10 and 12 pixels was based on two and three field measurements, respectively. Shrub LAI was mapped through inversion of the empirical relationship between shrub fraction and field-measured shrub LAI. The assumption underlying this approach is the observation that the open tree canopy of Mer Bleue bog is "underlain" by shrub canopy, and the shadow produced by trees is also "underlain" by shrub canopy. Thus, the shrub fraction of a pixel is assumed to be the sum of the sunlit vascular plant canopy and shadow fractions, i.e. [1 − sunlit *Sphagnum* moss fraction] (Fig. 5). Both approaches to map tree and shrub LAI based on fractions obtained from SMA and MESMA were validated using "leave-one-out"-cross-validation (LOOC) (Isaaks & Srivastava, 1989).

Our approach to map shrub LAI based on shrub fraction is not applicable to shrubs under the mixed forest canopy due to the relatively high degree of crown closure. Therefore, shrub LAI for mixed forest pixels was set to a constant value of 2.50 (1.13), which is the average (S.D.) shrub LAI measured along transect mbt5. Due to the lack of field-measured LAI, cattail LAI was set to a constant maximum growing season value of 3.63 (M.-C. Bonneville, unpublished data).

3. Results and discussion

3.1. Field measurements

A summary of needle-to-shoot area ratios of tamarack growing at Mer Bleue bog under two different lighting conditions is provided in Table 2. To the best of our knowledge, there has been no study reporting estimates of γ_E for tamarack.

Table 2
Needle-to-shoot area ratios (γ_E) of tamarack at Mer Bleue bog, growing under two different growth conditions in terms of light availability

Sample	Open bog		Forested bog	
	Mean	S.D.	Mean	S.D.
DT	1.56	0.34	1.33	0.27
DM	0.97	0.32	1.57	0.22
DL	1.78	0.86	1.53	0.39
MT	1.70	0.45	1.41	0.51
MM	1.49	0.16	1.55	0.06
ML	1.21	0.32	1.50	0.30
ST	1.04	0.17	1.06	0.70
SM	1.35	0.35	1.73	0.74
SL	1.37	0.34	1.34	0.28
Mean	1.39	0.38	1.45	0.38

For each growth condition, 45 shoot samples were taken from three trees: one dominant (D), one co-dominant (M), and one suppressed (S) tree, at three different height levels: top (T), middle (M), and bottom (L), resulting in nine classes with five shoots samples each: DT, DM, DL, MT, MM, ML, MS, ST, SM, and SL.

Table 3
Mer Bleue bog-specific clumping indices (Ω_E) of black spruce and tamarack and woody-to-total area ratios (α) of tamarack for use in Eq. (1) to derive LAI from LAI_e after Chen et al. (1997)

Parameter	Method	Tree species	No. of samples	Min.	Max.	Mean
Ω_E	TRAC	Black spruce	4	0.77	0.96	0.87
Ω_E	TRAC	Tamarack	4	0.77	0.95	0.87
α	Morphological measurements	Tamarack	12	0.12	0.17	0.15
α	Leaf-off LAI-2000 measurements	Tamarack	7	0.19	0.37	0.30

Comparisons of Table 2 with published estimates of γ_E for several coniferous tree species in Canada show that the mean values for tamarack under both growth conditions are considerably smaller. Chen et al. (2006) reported γ_E estimates of 1.66, 1.61, 1.71, and 1.91 for a mature and young Douglas fir stand on Vancouver Island, a balsam fir stand in New Brunswick, and a white pine stand in southern Ontario, respectively. The variation of γ_E among the two different growth conditions and also among the nine classes of each growth condition does not show any pattern. This is in contrast to the systematic variation of γ_E observed for different coniferous tree species among the nine classes by Chen et al. (2006), with the highest values for γ_E in dominant trees, followed by co-dominant and suppressed trees, respectively. Within a tree they reported generally higher γ_E values for shoots at higher levels than for shoots at lower levels. Considering the harsh growth conditions in acidic and nutrient-poor ombrotrophic peatlands, our generally small γ_E estimates for tamarack compared to the values reported by Chen et al. (2006) and the lack of any systematic variation between different height levels within trees is consistent with their hypothesis that the needle-to-shoot area ratio is mainly determined by growth conditions. Furthermore, our uniform γ_E estimates reflect the openness of the tree canopy at Mer Bleue bog where inter-tree shading does not result in more favorable lighting conditions of more open areas when compared to denser tamarack stands (Gower & Richards, 1990). For the calculation of tree LAI from LAI_e using Eq. (1) after Chen et al. (1997) we used the average γ_E value between open and forested bog of 1.42 (Table 2).

Our Mer Bleue bog-specific mean Ω_E estimate for black spruce of 0.87 is in reasonable agreement with the values provided by Chen et al. (2006) for the same species at two forest sites in Canada. Similar to the needle-to-shoot area ratio for tamarack reported above, there has been no study reporting Ω_E and α estimates for tamarack (Table 3). Our mean Ω_E estimate for tamarack is the same as for black spruce, i.e. reflecting a relatively high degree of foliage clumping.

The quick and reliable non-destructive estimation of α is still in its infancy, and often best estimates for this parameter are used in Eq. (1) (Chen et al., 2006). To reduce the considerable amount of uncertainty introduced by applying best estimates, we determined α with two simple non-destructive methods providing contrasting results (Table 3). Our α estimate of 0.15 based on morphological measurements is in the lower range compared to α

Table 4
Summary of field-measured tree and shrub LAI summarized according to the relative location of each transect on the subset of Landsat TM scene

	Tree LAI [m^2/m^2]	Shrub LAI (forested bog) [m^2/m^2]	Shrub LAI (open bog) [m^2/m^2]
No. of pixels	17	15	14
Min. LAI	0.23	0.76	0.73
Max. LAI	3.06	2.87	3.05
Mean LAI	1.59	1.57	1.50
S.D.	0.83	0.61	0.67

estimates reported by Chen et al. (2006) for other coniferous tree species in Canada, whereas an α estimate of 0.30 is in the higher range. We assume that the α estimate based on morphological measurements is underestimated due to the nature of the approach of simply using mean values of a few morphological measurements. Our α estimate based on leaf-off LAI-2000 measurements is most likely overestimated due to the timing of the non-growing season LAI-2000 measurement at dusk after a sunny day in mid-November. The short sunset provided us just with a very short time window with diffuse light conditions to take the measurements. The highest individual α values coincide with the last measurements when it was probably too dark, resulting in an overestimation of non-growing season LAI_e and thus α. We assume that our two contrasting α estimates define the limits of its actual mean value, and thus we used the average of both estimates of 0.225 for application in Eq. (1).

The final averaged tree and shrub LAI values per pixel after correcting LAI_e for γ_E, Ω_E, and α (tree LAI) and for α (shrub LAI) with Eqs. (1) and (2), respectively, are provided in Table 4. Tree LAI varies over a wide range from 0.23 and 3.06, resulting in a mean value of 1.59. This average tree LAI is much smaller than the average tree LAI of several forest sites in Canada (Chen et al., 2006), and thus reflects the low productivity of acidic and nutrient-poor ombrotrophic peatlands. Shrub LAI varies over a range similar to tree LAI, with a slightly lower mean shrub LAI measured along transects located in open areas of the bog compared to forested portions. The similar ranges and means of tree and shrub LAI, respectively, provided by Table 4 indicate the importance of the shrub canopy in the Mer Bleue bog's hydrological and ecological functioning as described in several studies (e.g., Lafleur et al., 2005; Moore et al., 2002).

3.2. Spectral vegetation indices for Mer Bleue

All three SVI computed from the atmospherically corrected Landsat TM subset of Fig. 3 respond to the dense tree canopy along drainage ditches and the beaver ponds with the highest values for Mer Bleue (Fig. 6). Non-vegetation pixels yield the lowest values for the respective SVI (e.g., the southern beaver pond of the northern finger delineating Mer Bleue bog, portions of the drainage dissecting the eastern half of Mer Bleue bog). Intermediate between these two extremes are the cattail marshes and areas of Mer Bleue bog characterized by pristine species composition and vertical vegetation structure. The central part of Mer Bleue bog, in particular, responds with values for the respective SVI similar to non-vegetation pixels, thus indicating sparse vascular vegetation. However, from field observations and aerial photographs (data not shown) we know that these central areas comprise very open patches of typical black spruce and tamarack canopies over an also relatively open and low shrub canopy. Thus, in these areas, the major contributor to background reflectance is the *Sphagnum* moss ground cover, with spectral features that do not allow for the adequate characterization of the absorption in the red portion of the visible range and the high reflectance of the NIR range of the vascular plants (Fig. 8).

The linear OLS regression relationships between the SVI of Fig. 6 and the field-measured tree and shrub LAI (open bog) of Table 4 are provided by Fig. 7. Regarding tree LAI, the highest value for R^2 is obtained for RSR ($R^2=0.27$), followed by SR ($R^2=0.13$) and NDVI ($R^2=0.09$), respectively. Generally, the R^2 values for the Mer Bleue bog are significantly smaller than those obtained in boreal forest ecosystems (e.g., Brown et al., 2000; Chen et al., 2002), indicating for each pixel that there is no single SVI vs. tree LAI linear regression relationship but a set of relationships, all of which are a function of crown closure and thus of the nature

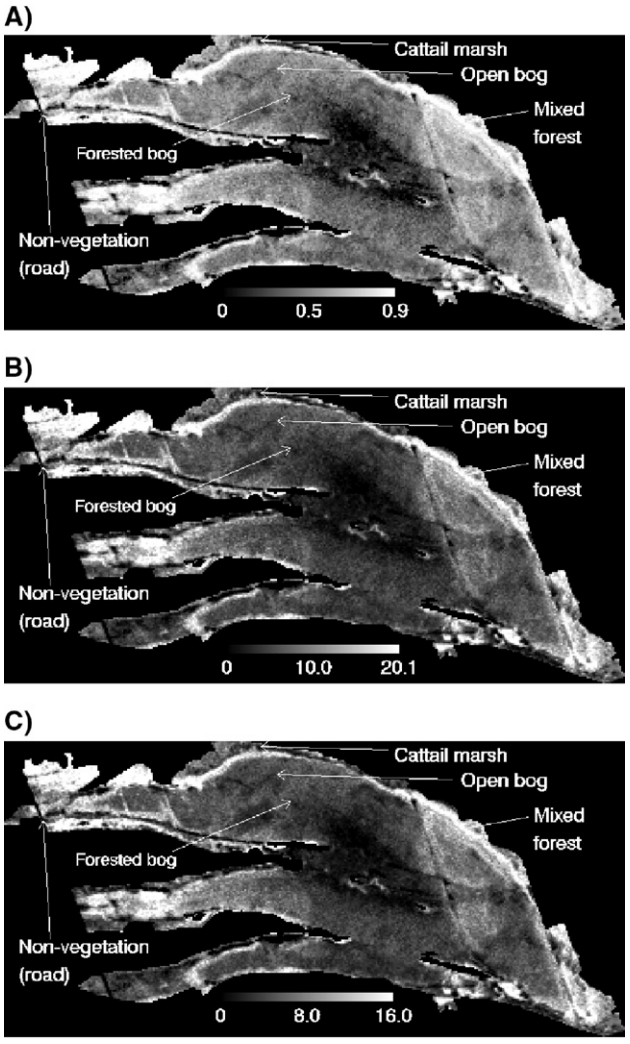

Fig. 6. Mapped SVI for Mer Bleue computed from the atmospherically corrected Landsat TM subset: (A) NDVI, (B) SR, and (C) RSR.

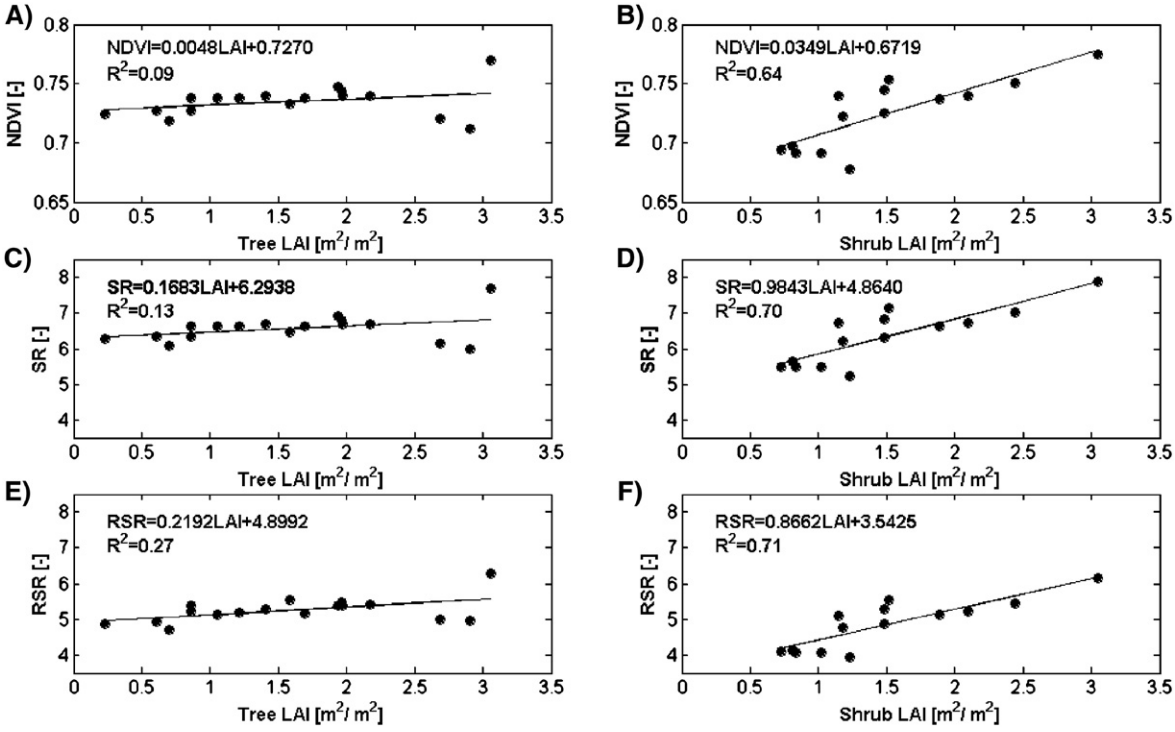

Fig. 7. Linear OLS regression relationships between SVI (Fig. 6) and field-measured tree and shrub LAI: A) NDVI vs. tree LAI, B) NDVI vs. shrub LAI, C) SR vs. tree LAI, D) SR vs. shrub LAI, E) RSR vs. tree LAI, and F) RSR vs. tree LAI.

of background reflectance. However, the general superiority of RSR over SR and NDVI for tree LAI mapping in boreal forests due to its capability to compensate for differences in canopy closure and background reflectance was demonstrated in several previous studies (e.g., Brown et al., 2000; Chen et al., 2002). For shrub LAI, the highest value for R^2 is again obtained for RSR ($R^2=0.71$), followed by SR ($R^2=0.70$) and NDVI ($R^2=0.64$), respectively. These significantly higher R^2 values for all three SVI demonstrate their general applicability to the shrub canopy of the open portions of the Mer Bleue bog. However, none of the SVI of Fig. 7 allows for mapping of shrub LAI of the forested portions of Mer Bleue bog.

3.3. Mixture decomposition with SMA and MESMA

We used nine *Sphagnum* moss reflectance spectra measured at Mer Bleue bog convolved to the wavelength range corresponding to the Landsat TM bands 1 through 5 for mixture

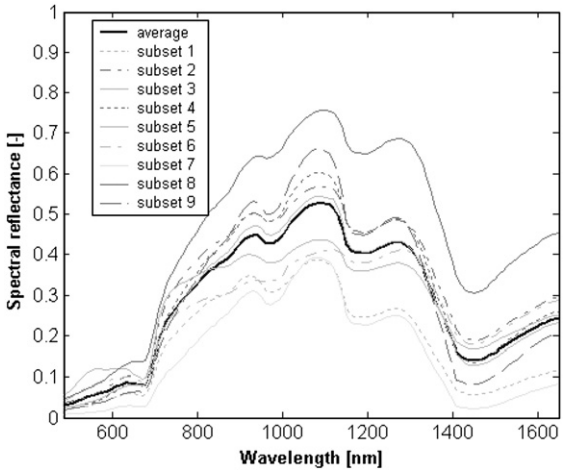

Fig. 8. *Sphagnum* moss reflectance spectra measured at Mer Bleue bog: nine individual sample sets for mixture decomposition with MESMA, and their average (bold line) for mixture decomposition with SMA.

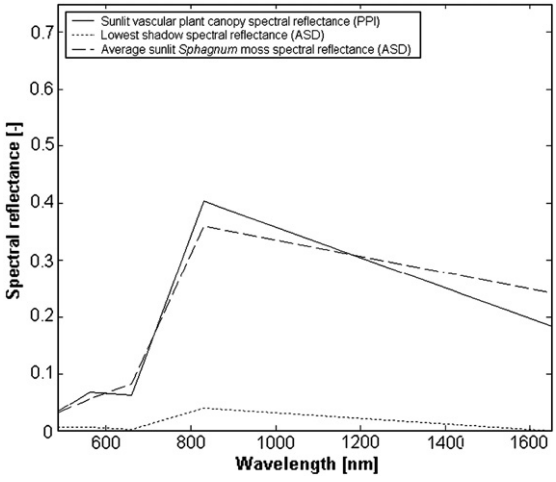

Fig. 9. Spectral characterization of the three-endmember model for mixture decomposition with SMA (convolved to the mid-points of the Landsat bands 1 through 5): sunlit vascular plant canopy, sunlit *Sphagnum* moss, and shadow.

decomposition (Fig. 8). All nine reflectance spectra are characterized by diagnostic reflectance differences in the visible, NIR, and SWIR distinguishing them from the reflectance spectra of vascular plants. Generally, *Sphagnum* moss is more reflective in the red portion of the visible range and less reflective in the NIR range than vascular plants. Further characteristic features of *Sphagnum* moss reflectance spectra described by Bubier et al. (1997) are the strong water absorption features at about 980 and 1200 nm, resulting in three distinctive spectral reflectance peaks at about 930, 1100, and 1300 nm (Fig. 8). However, the amplitudes of this general behavior varies over a wide range since it is significantly controlled by the near-surface volumetric moss moisture content, soil and water chemistry, and environmental conditions such as light availability (Bryant & Baird, 2003; Bubier et al., 1997; Harris et al., 2005, 2006).

We used the average of the nine *Sphagnum* moss reflectance spectra of Fig. 8 to spectrally characterize the sunlit *Sphagnum* moss endmember of our three-endmember model for SMA. For the spectral characterization of the shadow endmember, we

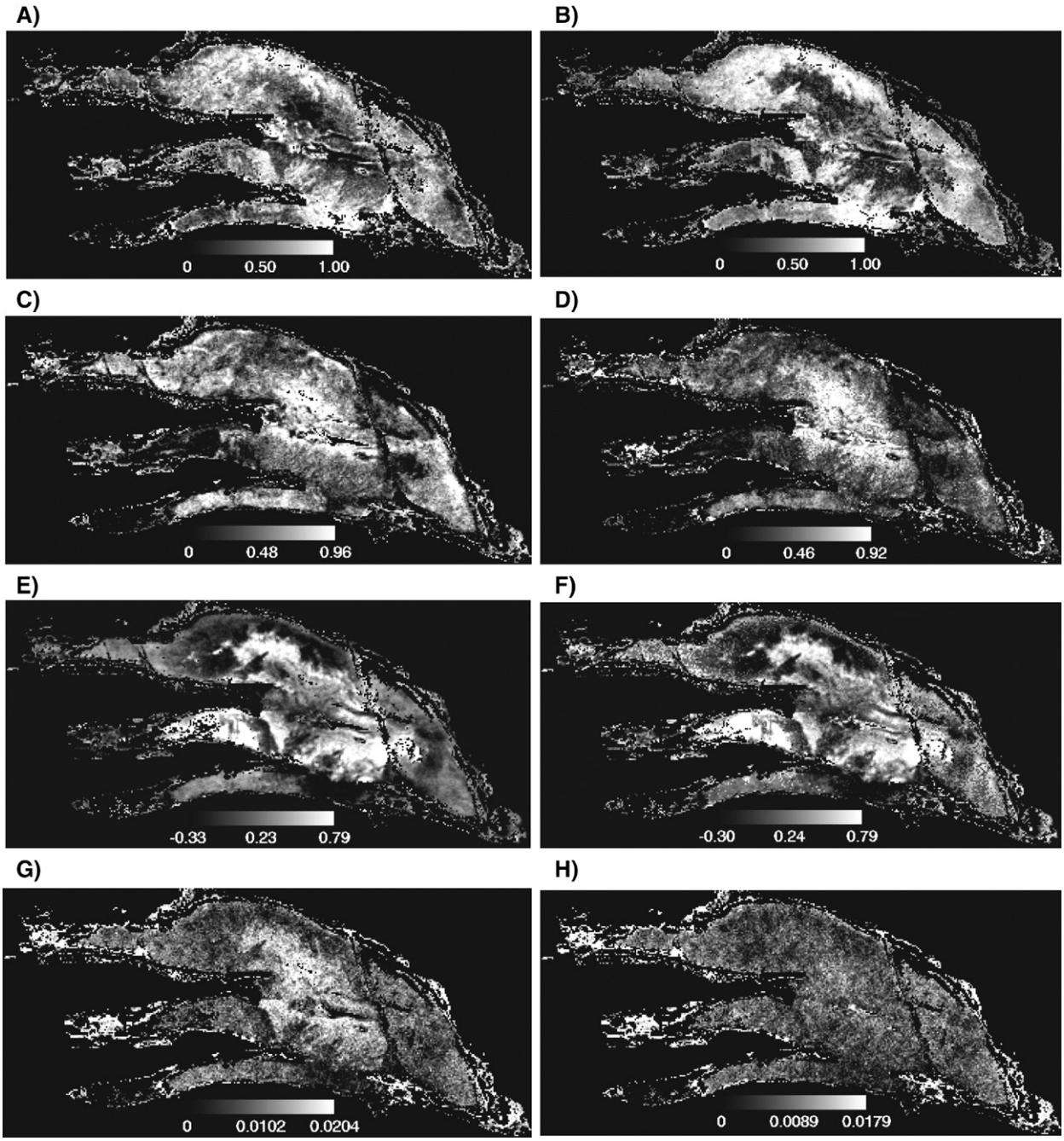

Fig. 10. Fractions and assessment of model fit for SMA and MESMA: A) sunlit vascular plant endmember (SMA), B) sunlit vascular plant endmember (MESMA), C) sunlit *Sphagnum* moss endmember (SMA), D) sunlit *Sphagnum* moss endmember (MESMA), E) shadow endmember (SMA), F) shadow endmember (MESMA), G) RMSE (SMA), and H) RMSE (MESMA).

Table 5
Direct comparison of the classified Mer Bleue subsets obtained with SMA and MESMA (subset of Fig. 8)

Mer Bleue # pixels	29,734	
Non-pristine (Fig. 4) # pixel	9856	
Mer Bleue bog # pixels (%)	19,878 (100)	
	SMA	MESMA
Average reflectance spectra # pixels (%)	19,393 (97.56)	–
Classified # pixels (%) ss 1	–	19 (0.10)
Classified # pixels (%) ss 2	–	172 (0.87)
Classified # pixels (%) ss 3	–	3720 (18.71)
Classified # pixels (%) ss 4	–	1439 (7.24)
Classified # pixels (%) ss 5	–	8 (0.04)
Classified # pixels (%) ss 6	–	9104 (45.80)
Classified # pixels (%) ss 8	–	5119 (25.75)
Classified # pixels (%) ss 9	–	130 (0.65)
Total # pixels (%)	19,393 (97.56)	19,711(99.16)

manually selected the field-measured shadow reflectance spectrum with the lowest spectral reflectance values in the visible, NIR, and SWIR ranges. The sunlit vascular plant canopy endmember was spectrally characterized through the combined use of MNF and PPI. The resulting sunlit vascular plant canopy reflectance spectrum is similar to the sunlit *Sphagnum* moss reflectance spectrum, indicating the influence of the underlying *Sphagnum* moss ground cover on the overall spectral response of the shrub canopy (Fig. 9).

For MESMA we built a spectral library that consisted of all nine *Sphagnum* moss reflectance spectra (Fig. 8) together with the sunlit vascular plant canopy and shadow endmembers (Fig. 9) resulting in nine different three-endmember models.

The fractions of the three endmembers and the RMSE obtained from mixture decomposition with SMA and MESMA, respectively, are provided in Fig. 10. For both mixture decomposition approaches, the distributions of the sunlit vascular plant canopy endmember are relatively uniform (Fig. 10A and B, respectively). The highest sunlit vascular plant canopy fractions are south of the northern margin and north of the southern margin of Mer Bleue bog corresponding to open bogs where trees are absent (Fig. 3). The lowest values occur in the central, forested portions of Mer Bleue bog. This portion of the bog also shows the lowest response to the SVI (Fig. 6), indicating sparse vascular vegetation.

The spatial distributions of the sunlit *Sphagnum* moss endmember (Fig. 10C and D, respectively) are the inverse of the sunlit vascular plant canopy endmember, i.e. relatively uniform except for the central portions, where the highest fractions occur. High sunlit *Sphagnum* moss fractions are indicative of the absence or a low density of the shrub canopy. The shadow fractions from SMA and MESMA both show a clear pattern corresponding to open and forested portions of the Mer Bleue bog (Fig. 10E and F, respectively): areas where trees are absent or that just contain individual, isolated trees are characterized by the lowest shadow fractions, whereas forested portions are characterized by the highest shadow fractions. Seventy pixels in Fig. 10E and 66 pixels in Fig. 10F have unrealistic negative shadow fractions, some of which occur in both images. However, since these pixels were all located in areas of Mer Bleue that clearly correspond to cattail marsh, mixed forest, or non-vegetation they were excluded from the subsequent analysis. Most likely these pixels were simply misclassified by SAM.

Regarding the spatial distributions of RMSE, for both SMA and MESMA the highest values occur in areas of Mer Bleue that correspond to cattail marsh, mixed forest, or non-vegetation (Fig. 10G and H, respectively), and thus were most likely also misclassified by SAM. However, since these pixels have realistic fractions, they were kept for the subsequent analysis. Within the Mer Bleue bog, RMSE obtained from SMA covers a wider range and shows more spatial variation than RMSE obtained from MESMA. The highest RMSE values from SMA occur in the central areas of the bog, which also show the highest sunlit *Sphagnum* moss and shadow fractions.

The direct comparison of the classified Mer Bleue subsets obtained with SMA and MESMA is summarized in Table 5. SMA using the average *Sphagnum* moss reflectance spectra of Fig. 8 can be used to model the spectral response of 97.56% of the pixels of the Mer Bleue subset, whereas MESMA using all nine *Sphagnum* moss reflectance spectra successfully models 99.16%.

The spatial variation of the different *Sphagnum* moss reflectance spectra of Fig. 8 used by MESMA shows that different areas of the Mer Bleue bog are modeled best by different three-endmember models (Fig. 11). For example, the spectral response of forested central portions of the bog is modeled best with a three-endmember model that includes subset 8 in Fig. 8, whereas the open portions of the bog are modeled best with a three end-member model that includes subset 6. Other subsets in Fig. 8 such as subsets 1, 2, and 9 are of minor importance, the three-endmember model that includes subset 7 is not used at all (Table 5).

Qualitatively, the spatial distributions of all three endmembers in Fig. 10 obtained from SMA and MESMA, respectively, are good approximations of the spatially varying pristine species composition and vertical vegetation structure of Mer Bleue bog, thus indicating the general applicability of our three end-member model to ombrotrophic peatlands. However, the spatial variability and the greater range of RMSE obtained from SMA compared to MESMA, and the lower percentage of classified pixels indicate that the widely varying spectral characteristics of the sunlit *Sphagnum* moss endmember are not adequately described by the average *Sphagnum* moss reflectance spectrum of Fig. 8, which might result in

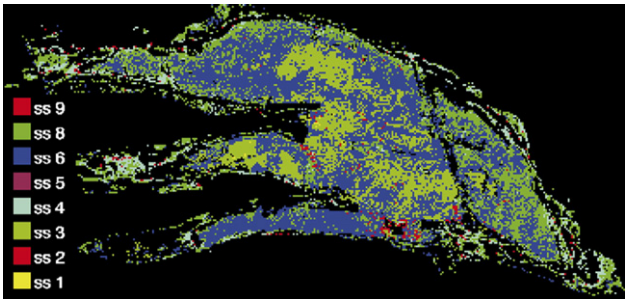

Fig. 11. Classified Mer Bleue subset (MESMA) using the nine reflectance spectra in Fig. 8 to describe the sunlit *Sphagnum* moss endmember (ss = subset of Fig. 8).

less accurate fractions. Furthermore, by using a range of different *Sphagnum* moss reflectance spectra, the influence of the similarity between the average sunlit *Sphagnum* moss and the sunlit vascular plant canopy reflectance spectra is minimized (Fig. 9). Less accurate fractions limit the use of SMA for peatland LAI mapping as demonstrated in Section 3.5.

3.4. Geometric-optical radiative transfer modeling

The simulated relationship between shadow fraction and tree LAI is clearly not linear but appears to be of exponential nature and is best described with a nonlinear exponential equation of the general form (Fig. 12):

$$y = a - b * \exp^{(-x/c)} \quad (6)$$

where x and y are tree LAI and shadow fractions, respectively, and a, b, and c are regression constants. The constants a, b, and c of Eq. (6) describe the simulated exponential relationship between tree LAI and shadow fraction and were determined through unconstrained, non-linear OLS regression analysis as 0.361, 0.326, and 1.698, respectively (Fig. 12).

The first constant in Eq. (6), a, is the maximum shadow fraction, and the second constant, b, is the difference between maximum shadow fraction and background shadow, i.e. shadow produced by the shrub canopy, since no trees are present at a tree LAI value of zero. Thus, for our simulated relationship the amount of shadow produced by the shrub canopy is estimated as 0.035.

3.5. Tree and shrub LAI mapping using MESMA

Based on Eq. (6) we determined the regression relationships between tree LAI (Table 4) and shadow fractions obtained from SMA (Fig. 10E) and MESMA (Fig. 10F), respectively, through partially constrained non-linear OLS regression analysis (Fig. 13A and B, respectively). In both the regression relationships of Fig. 13A and B the first regression constant, a, was preset to the maximum shadow fraction obtained from mixture decomposition (Fig. 10E and F, respectively). The second regression constant, b, was pre-set to the difference of the first regression constant and background shadow. An average background shadow of 0.09 produced by the shrub canopy was calculated based on pixels corresponding to the three shrub transects mbs1, mbs2, and mbs3 located in open areas of the Mer Bleue bog where trees were absent. The third regression constant, c, was determined iteratively through the regression analysis. Comparison of the R^2 values obtained through the mixture decomposition-based non-linear OLS regression (Fig. 13A and B, respectively) with those from the SVI-based linear OLS regression (Fig. 7A, C, and E, respectively) reveals that the shadow fraction is generally a strong predictor of tree LAI in ombrotrophic peatlands, with MESMA being superior over SMA as indicated by R^2 values of 0.75 (Fig. 13B) and 0.61 (Fig. 13A), respectively. Similar findings demonstrating the general superiority of the shadow fraction over SVI for tree LAI estimation were made by Hall et al. (1995) and Hall et al. (2003).

For the estimation of shrub LAI based on shrub fraction we also applied the approach of partially constrained non-linear OLS regression analysis using Eq. (6) (Fig. 13C and D, respectively). A simple plot of field-measured shrub LAI and the shrub fractions obtained from SMA and MESMA revealed that the shrub fraction reaches a plateau at about 0.90 despite increasing shrub LAI. A possible reason for this might be that increasing shrub LAI is inherent with increasing shrub fraction up to a certain point, after which shrub LAI increases as a function of shrub height resulting in more foliage seen by the LAI-2000 instrument sensor but not necessarily in a higher fraction of shrubs covering the ground as determined through SMA and MESMA, respectively. This interpretation is supported by the observation that the highest shrub LAI values along our transects were measured at mbt5 and mbs3, both of which are close to a drainage ditch and to the margin of Mer Bleue bog, respectively. Both areas are characterized by lower water table positions with more favorable growth conditions, resulting in higher and denser shrub canopies. In both OLS regression relationships of Fig. 13C and D, respectively, the first regression constant, a, was pre-set to a maximum shrub fraction of 0.90, representing the plateau of the exponential relationship. The background was set to zero, since if shrubs are absent, shrub LAI is supposed to equal zero. Our simple approach of calculating the shrub fraction as the sum of the sunlit vascular plant canopy and the shadow fraction (i.e. [1 − sunlit *Sphagnum* moss fraction]) most likely resulted in overestimation of the shrub fraction for some areas of Mer Bleue bog since it does not account for the situation where shadows produced by trees are "underlain" directly by *Sphagnum* moss, i.e. where the shrub canopy is absent. However, we assume that this overestimation is on average balanced by the underestimation that would result from the correction of 0.09 to the shadow fraction for the average shadow produced by the shrub canopy estimated above. Simple comparison of the R^2 values obtained through the mixture decomposition-based non-linear OLS regression (Fig. 13C and D, respectively) with those from the SVI-based linear OLS regression (Fig. 7B, D, and F, respectively) might suggest that

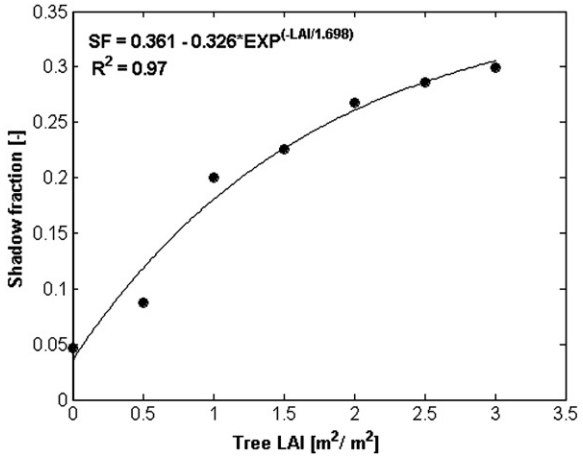

Fig. 12. Simulated exponential relationship between shadow fraction (SF) and tree LAI for a Landsat TM pixel of Mer Bleue bog.

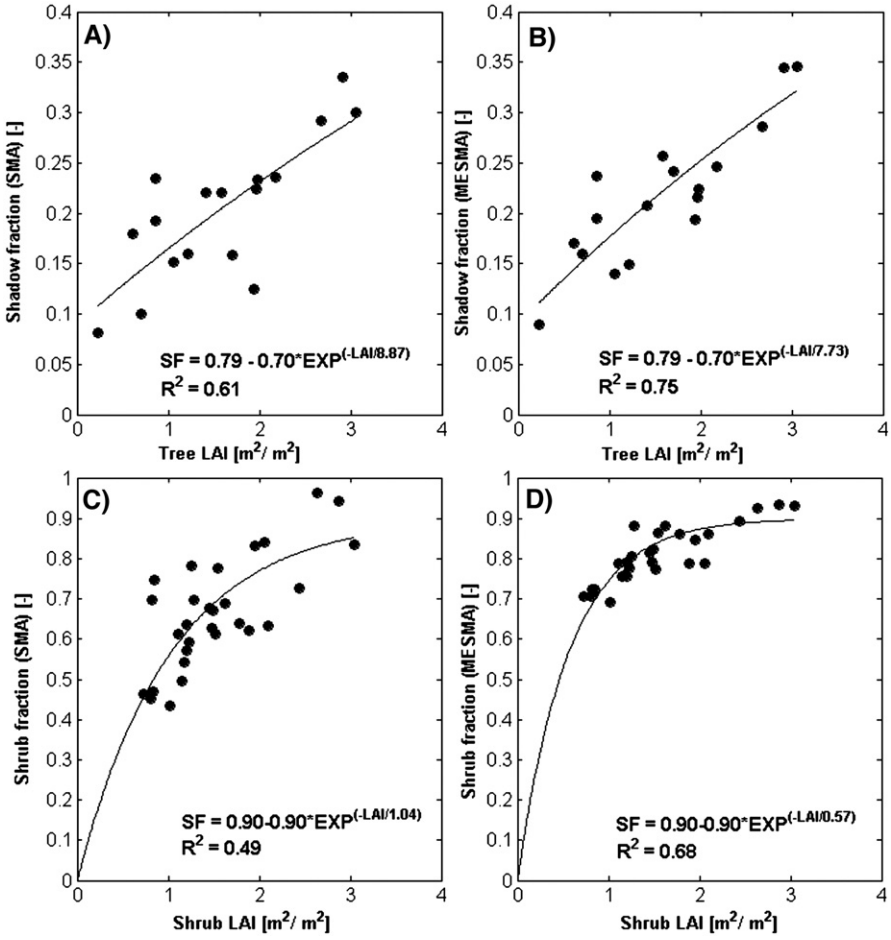

Fig. 13. Exponential relationships between shadow fractions derived from SMA and MESMA, respectively, and field-measured tree LAI based on Eq. (6), and between shrub fractions derived from SMA and MESMA, respectively, and field-measured shrub LAI, also based on Eq. (6).

the three SVI are generally stronger predictors of shrub LAI than the shrub fraction. However, SVI-based shrub LAI mapping produces good results in open portions of the Mer Bleue bog but fails in its forested portions since these SVI respond to both shrub and tree canopies due to the low degree of canopy closure. Our approach based on shrub fraction is not sensitive to canopy closure, thus allowing for shrub LAI mapping in Mer Bleue bog's open and forested portions, and still produces acceptable results (Fig. 13C and D, respectively). Similar to tree LAI, MESMA is again superior over SMA as indicated by R^2 values of 0.68 (Fig. 13D) and 0.49 (Fig. 13C), respectively.

3.6. Cross-validation

To gain confidence in our approaches we tested the tree and shrub LAI predictors derived from the shadow (Fig. 13A and B, respectively) and shrub fractions (Fig. 13C and D, respectively) with LOOC for the pixels of the tree and shrub transects. For tree LAI, as expected, the shadow fraction from MESMA (Fig. 14B) results in more accurate tree LAI estimates with R^2 and RMSE values of 0.74 and 0.48, respectively, compared to tree LAI estimates based on SMA (Fig. 14A) with R^2 and RMSE values of 0.60 and 0.62, respectively. For both SMA and MESMA, the slope and intercept are not significantly different from 1 and 0 (significance level = 0.05), respectively.

Similar to tree LAI estimates, shrub LAI estimates based on the shrub fraction from MESMA (Fig. 14D) with R^2 and RMSE values of 0.68 and 0.42, respectively, are more accurate than shrub LAI estimates based on the shrub fraction from SMA (Fig. 14C) with R^2 and RMSE values of 0.55 and 0.73, respectively. The shrub LAI predictor based on shrub fraction obtained from SMA tends to overestimate shrub LAI in the higher range even though slope and intercept are not significantly different from 1 and 0 (significance level = 0.05), respectively. Shrub LAI estimates based on MESMA are slightly underestimated at higher shrub LAI values and slightly overestimated at lower shrub LAI values with the slope just slightly different from 1 ($p = 0.0417$) and the intercept not significantly different from 0 (significance level = 0.05).

For the final production of the tree and shrub LAI maps for Mer Bleue based on inversion of Eq. (6), the shadow and sunlit *Sphagnum* moss (i.e. [1 − sunlit *Sphagnum* moss]) fractions determined with MESMA were used (Fig. 15A–C). For the tree LAI calculation of the mixed forest pixels (Fig. 4) with Eq. (5) we constrained the RSR values of Fig. 6C to a maximum value of 9.2 (i.e. 29.47% of the mixed forest pixels). For the shrub

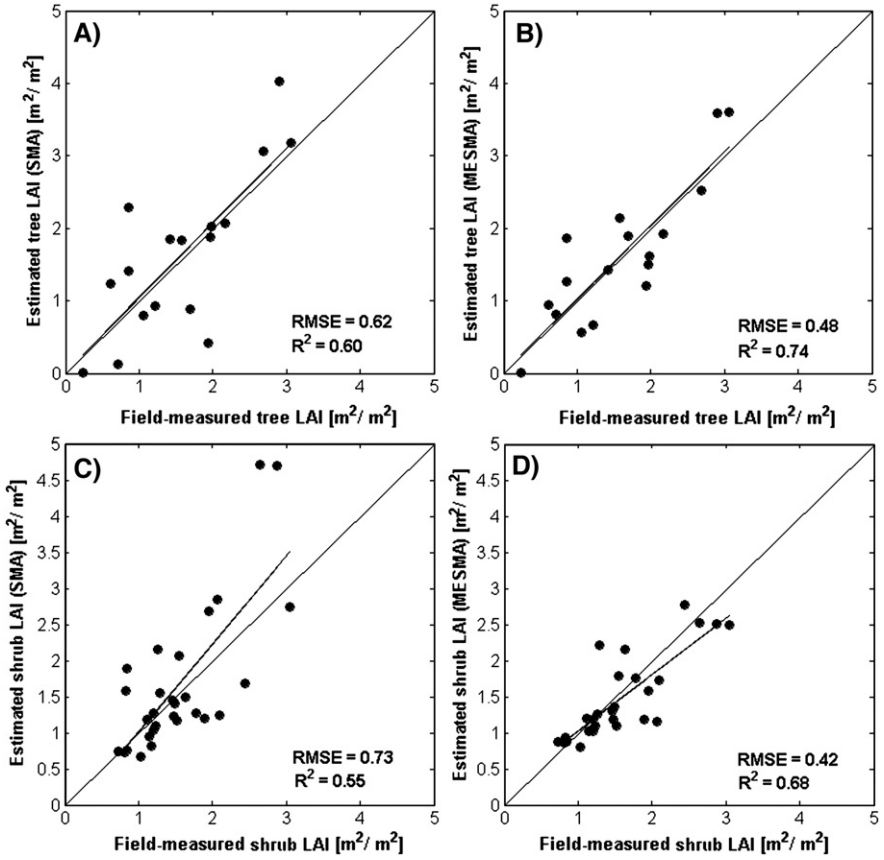

Fig. 14. "Leave-one-out"-cross-validation (LOOC) for tree LAI estimated based on shadow fraction obtained from SMA (A) and MESMA (B), and for shrub LAI estimated based on shrub fraction obtained from SMA (C) and MESMA (D).

LAI calculation with Eq. (6) based on Fig. 10F, we constrained the shrub fraction of a pixel to a maximum value of 0.89 (i.e. 9.34% of Mer Bleue bog). We consider this constraint to be reasonable since at Mer Bleue bog a shrub fraction greater than 0.90 over an area of 900 m^2 is unrealistic due to the bog's microtopography. On average, hollows, which make up approximately one third of Mer Bleue bog's surface area (Lafleur et al., 2005), have a percent cover of less than 0.5, and thus full shrub coverage over large areas does not exist (Sonnentag et al., in press).

Total LAI was calculated as the sum of tree and shrub LAI (Fig. 15C). In all three maps, non-vegetation pixels (Fig. 4), pixels that were excluded due to negative shadow fractions (Fig. 10F), and unclassified pixels (Fig. 11) were set to NoData. Qualitatively, the LAI maps of Fig. 15 capture the spatial variation of the species composition and vertical vegetation structure of Mer Bleue quite well when compared to Fig. 3. As expected, the highest total LAI values occur along beaver ponds and drainage ditches, whereas the Mer Bleue bog is characterized by considerably lower total LAI values. A striking feature of the shrub LAI map is the generally low shrub LAI values in the central forested parts of Mer Bleue bog as indicated by the fractions of Fig. 10 (Fig. 15B). The SVI of Fig. 6 indicate sparse vascular vegetation for these portions of the Mer Bleue bog, which would result in low total LAI values. However, the total LAI of these areas is in the same range as for the open portions of Mer Bleue bog, with the tree LAI as the major contributor to total LAI.

4. Conclusions

Tree LAI of forest ecosystem has routinely been mapped based on the empirical relationships between SVI derived from remote sensing imagery and LAI field measurements. The suitability of this approach is limited for tree and shrub LAI mapping in ombrotrophic peatlands, mainly due to the spatially varying vegetation structure of their multi-layer canopy, which usually includes a moss ground cover. Additionally, mosses have spectral characteristics that are significantly different from vascular plants.

Based on a promising approach to map tree LAI in forest ecosystems using fractions from mixture decomposition with SMA, we mapped tree and shrub LAI of an ombrotrophic peatland at the peak growing season. Applying MESMA, an extension of SMA, to a three-endmember model comprising a general sunlit vascular plant canopy, *Sphagnum* moss, and shadow, the widely varying spectral characteristics of *Sphagnum* mosses were taken into account in the mixture decomposition. A slightly higher percentage of pixels of the Mer Bleue bog were successfully unmixed by our three endmember model with MESMA than with SMA. Furthermore, mixture decomposition with MESMA reduces the RMSE, mainly in portions

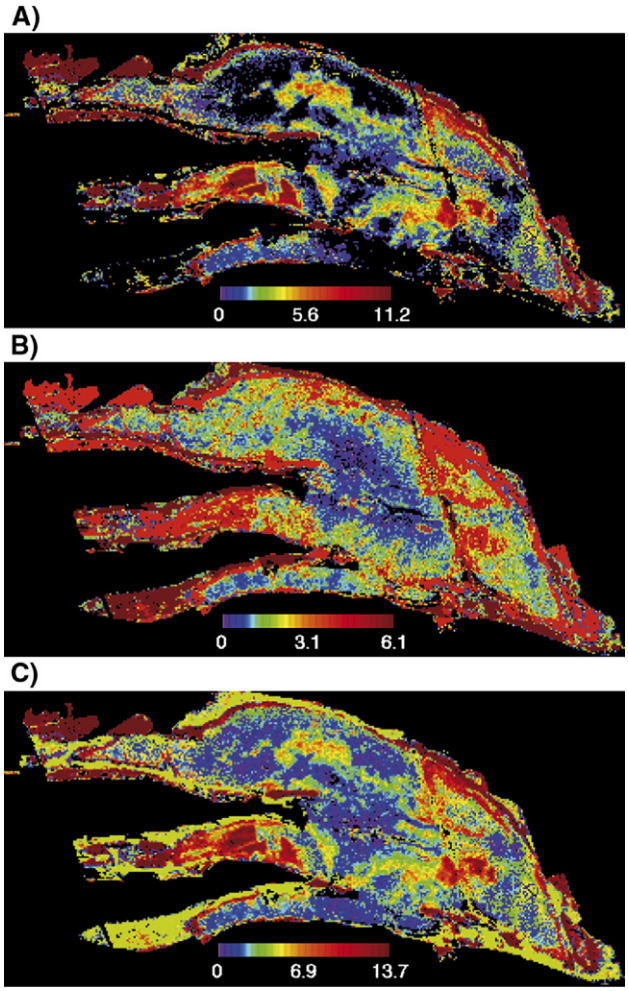

Fig. 15. Mapped LAI for Mer Bleue based on fractions obtained from MESMA and Chen et al. (2002): tree LAI (A), shrub LAI (B), and total LAI (C).

of Mer Bleue bog where the shrub canopy is sparse or absent and the overall pixel spectral signature is mainly controlled by the spectral characteristics of *Sphagnum* mosses. Thus, it can be assumed that the fractions obtained from MESMA are more accurate than the fractions obtained from SMA.

The nature of the exponential relationship between shadow fraction and tree LAI in peatlands shows that a small portion of the shadow fraction has to be attributed to the shrub canopy. Validation with LOOC shows that less accurate fractions from SMA than from MESMA result in weaker predictions of both tree and shrub LAI.

We are confident that our approach developed for the multi-layer canopy of an ombrotrophic peatland can be used successfully to map tree and shrub LAI in similar ecosystems. For example, another common type of peatland includes fens, which receive, in addition to precipitation, hydrological inputs from their surrounding mineral uplands in the form of surface and subsurface flow (minerotrophic). As a result, fens, commonly subdivided into poor and rich fens, are less acidic and nutrient-rich peatlands, dominated by feather mosses, graminoids, shrubs, and coniferous and deciduous trees (Wheeler & Proctor, 2000). Future research should investigate the applicability of our approach to the multi-layer canopy of minerotrophic peatlands, and also its applicability to a larger area containing both, ombrotrophic and minerotrophic peatlands. Furthermore, the applicability of the resulting LAI maps for the explicit parameterization of two distinct canopy layers in distributed, process-oriented ecosystem models still has to be explored.

Acknowledgement

We thank Sylvain Leblanc (Canada Centre for Remote Sensing, Ottawa) for sharing his latest version of 4-Scale, Marie-Claude Bonneville (McGill University, Montreal) for her cattail marsh picture, Prof. Ian Strachan (McGill University, Montreal) for providing us with the LAI-2000 instrument, and Prof. Jonathan Seaquist (McGill University, Montreal) for insightful comments and suggestions. We also thank the three anonymous reviewers for their careful reading and helpful comments on an earlier draft of this manuscript. The Mer Bleue boundary vector dataset was kindly provided by Gershon Rother (National Capital Commission, Ottawa). This work was supported by the Fluxnet Canada Research Network funded by the Natural Science and Engineering Council of Canada, the Canadian Foundation of Climate and Atmospheric Sciences and BIOCAP Canada.

Appendix A

For 12 tamarack trees we measured height, diameter at breast height (DBH), and average branch length at three different height levels (top, middle, and bottom), and counted the number of branches of the entire tree. For three representative branches corresponding to the average length of each height level we counted the number of twigs, and measured their lengths and radii at the stem and at the end. Based on these measurements we calculated the woody surface area (A_W) of each tree as the sum of stem surface area (A_S), average branch surface area (A_B), and average twig surface area (A_T). A_S and A_T were calculated as the lateral surface area of circular cylinders with:

$$A = 2\pi rh \qquad (A-1)$$

where r is stem radius [m] and an average twig radius of 0.002 m, respectively, and h is tree height [m] and twig length [m], respectively. A_B was calculated by equally dividing the total number of branches into the three height levels and multiplying the number of branches with an average branch surface area of each height level, which was calculated as the surface area of truncated cones not including the top and the base circles, with:

$$A = \pi(r_1 + r_2)\sqrt{(r_1 - r_2)^2 + h^2} \qquad (A-2)$$

where r_1 and r_2 are average branch radii [m] at the stem and at the end, respectively, and h is average branch length [m] per

height level of each tree. The calculation of total tree leaf area (A_L) is based on a needle-to-woody area ratio ε, which we calculated based on the 90 tamarack shoot samples collected for the needle-to-shoot area estimation with:

$$\varepsilon = \frac{\sum A_N}{\sum A_T} \quad (A-3)$$

where A_N is half the total needle area (including all sides) in a shoot [m^2], and A_T is half the total woody area [m^2] of a shoot sample, i.e. half the surface area of its twig. A_T was calculated using Eq. (A-1) with the average twig radius of 0.002 m determined as part of the previous tree woody area calculation, and the twig length [m] of the respective shoot sample. Based on Eq. (A-3) we calculated an average value for ε of 11.69. The total needle surface area of each tree was calculated as the sum of the top, middle, and bottom level needle surface areas, which in turn were calculated by multiplying ε with the twig surface area of the respective height level as determined in the previous tree woody area calculation. Using A_W and A_N, we calculated an average value for α in accordance with Kucharik et al. (1998) with:

$$\alpha = \frac{\sum A_W}{\sum A_W + \sum A_N} \quad (A-4)$$

Appendix B

The geometric-optical radiative transfer model 4-Scale considers the interaction of light with architectural elements of tree canopies at four different scales: tree groups, tree crowns, branches, and foliage elements. To simulate the patchiness usually observed in boreal forests, 4-Scale uses a Neyman type A distribution, assuming that trees are combined in groups, with the center of the group entirely contained in quadrats that divide the simulation domain into smaller areas (Chen & Leblanc, 1997). A geometry-based multiple scattering scheme considers the scattering of light between all architectural canopy elements (Chen & Leblanc, 2001).

In our study we parameterized 4-Scale using averaged leaf scale western larch (*Larix occidentalis*) reflectance and transmittance spectra obtained as part of a previous study (D.A. Roberts, unpublished data). The leaf scale spectra were measured using a modified Beckman DK2A with an integrating sphere attachment designed for measurements of directional hemispherical transmittance or reflectance. Western larch spectra were collected from needles destructively sampled from the sunlit portions of lower tree crowns. After collection, needles were stored cooled and transported to the laboratory for spectral measurements. Spectra were collected within 48 h of original collection. Laboratory spectra were collected from needles arranged on slide mounts with minimal gaps and overlaps as described by Roberts et al. (2004). Regarding the optical properties of background, we parameterized 4-Scale using the average of nine sets of branch scale background reflectance spectra obtained in this study.

In addition to leaf and branch scale input reflectance spectra, 4-Scale requires several site- and tree architecture specific input parameters including tree LAI and stand density. To avoid the arbitrary variation of stand density with increasing tree LAI or the "growth" of bigger trees with less foliage by keeping stand density constant with increasing tree LAI, we determined the empirical relationship between stand density and tree LAI with unconstrained nonlinear OLS regression analysis for a total of nine flags of mbt3, mbt4, and mbt5.

Based on the exponential stand density vs. tree LAI relationship ($R^2 = 0.62$) we estimated stand densities corresponding to tree LAI values of 0.1, 0.5, 1.0, 1.5, 2.0, 2.5, and 3.0 (Table B-1). For comparison of simulated shadow fractions with shadow fractions derived from the subset of the Landsat TM scene with SMA and MESMA, the simulations were performed using a SZA corresponding to date and time of image acquisition and a viewing zenith angle (VZA) of 0°. Other parameters required by 4-Scale are based on field observations (stick and crown height, crown radius, and foliage element size) and measurements (clumping index, needle-to-shoot area ratio) obtained in this study, or are set following literature recommendations (number of quadrats, Neyman A grouping, and repulsion factor that avoids unnatural tree crown overlapping) after Chen and Leblanc (1997).

Based on the input spectra and the site- and tree architecture specific input parameters of Table B-1, 4-Scale calculates the spectral reflectance of the four domain components sunlit and shaded crown, and sunlit and shaded background, together with their respective fractions. The overall domain spectral reflectance is calculated by associating the spectral reflectance of the domain components with their fractions according to Eq. (3) without the residual error.

Table B-1: 4-Scale parameterizations used to investigate the nature of the empirical relationship between shadow fraction and tree LAI for Mer Bleue bog

	LAI	0.1	0.5	1	1.5	2	2.5	3
Site parameters	Size	900	900	900	900	900	900	900
	Stand density [trees/900 m^2]	64	64	153	294	354	380	391
Tree clumping	# Quadrats [-]	5	5	5	5	5	5	5
	Neyman A grouping [-]	2	2	2	2	2	2	2
Other	SZA [°]	43	43	43	43	43	43	43
	VZA [°]	0	0	0	0	0	0	0
	Stick height [m]	0.2	0.2	0.2	0.1	0.1	0.1	0.1
	Crown height [m]	1.7	1.7	1.7	1.1	1.1	1.1	1.1
	Crown radius [m]	0.7	0.4	0.4	0.3	0.3	0.3	0.3
	Clumping index [-]	0.87	0.87	0.87	0.87	0.87	0.87	0.87
	Apex angle [°]	13	13	13	13	13	13	13
	Needle-to-shoot area ratio [-]	1.41	1.41	1.41	1.41	1.41	1.41	1.41
	Foliage element size [m]	0.05	0.05	0.05	0.05	0.05	0.05	0.05
	Repulsion factor	0.5	0.5	0.5	0.5	0.5	0.5	0.5

References

Adams, J. N., Smith, M. O., & Gillespie, A. R. (1993). Imaging spectrometry: Interpretation based on spectral mixture analysis. In C. M. Pieters, & P. A. J. Englert (Eds.), *Remote geochemical analysis: Elemental and mineralogical composition* (pp. 145–166). Cambridge, England: Press Syndicate of University of Cambridge.

Baldocchi, D., Kelliher, F. M., Black, T. A., & Jarvis, P. G. (2000). Climate and vegetation controls on boreal zone energy exchange. *Global Change Biology*, *6*, 69–83.

Ballantine, J. -A. C., Okin, G. S., Prentiss, D. E., & Roberts, D. A. (2005). Mapping African landforms using continental scale unmixing of MODIS imagery. *Remote Sensing of Environment*, *97*, 470–483.

Barr, A. G., Black, T. A., Hogg, E. H., Kljun, N., Morgenstern, K., & Nesic, Z. (2004). Inter-annual variability in the leaf area index of a boreal aspen–hazelnut forest in relation to net ecosystem production. *Agricultural and Forest Meteorology*, *126*, 237–255.

Berterretche, M., Hudak, A. T., Cohen, W. B., Maiersperger, T. K., Gower, S. T., & Dungan, J. (2005). Comparison of regression and geostatistical methods for mapping leaf area index (LAI) with Landsat ETM+ over a boreal forest. *Remote Sensing of Environment*, *96*, 49–61.

Boardman, J. W., Kruse, F. A., & Green, R. O. (1995). Mapping target signatures via partial unmixing of AVIRIS data. *Summaries, 5th JPL Airborne Earth Science Workshop*, *Vol. 1*. (pp. 23–26)Pasadena, CA: Jet Propulsion Laboratory (JPL Publications 95-1).

Brown, L., Chen, J. M., Leblanc, S. G., & Cihlar, J. (2000). A shortwave infrared modification to the Simple Ratio for LAI retrieval in boreal forests: An image and model analysis. *Remote Sensing of Environment*, *71*, 16–25.

Bryant, R. G. (1996). Validated linear mixture modelling of Landsat TM data for mapping evaporate minerals on a playa surface: Methods and applications. *International Journal of Remote Sensing*, *17*, 315–330.

Bryant, R. G., & Baird, A. J. (2003). The spectral behaviour of *Sphagnum* canopies under varying hydrological conditions. *Geophysical Research Letters*, *30*, 1134–1138.

Bubier, J. L., Barrett, N. R., & Crill, P. M. (1997). Spectral reflectance measurements of boreal wetland and forest mosses. *Journal of Geophysical Research*, *102*(D24), 29483–29494.

Chen, J. M. (1996). Optically-based methods for measuring seasonal variation of leaf area index in boreal conifer stands. *Agricultural and Forest Meteorology*, *80*, 135–163.

Chen, J. M., & Black, T. A. (1992). Defining leaf area index for non-flat leaves. *Plant, Cell & Environment*, *15*, 421–429.

Chen, J. M., & Cihlar, J. (1995). Plant canopy gap size analysis theory for improving optical measurements of leaf area index. *Applied Optics*, *34*, 6211–6222.

Chen, J. M., & Cihlar, J. (1996). Retrieving leaf area index of boreal conifer forests using Landsat TM images. *Remote Sensing of Environment*, *55*, 153–162.

Chen, J. M., Govind, A., Sonnentag, O., Zhang, Y., Barr, A., & Amiro, B. (2006). Leaf area index measurements at Fluxnet Canada forest sites, FCRN special issue. *Agricultural and Forest Meteorology*, *140*, 257–268.

Chen, J. M., & Leblanc, S. G. (1997). A 4-Scale bidirectional reflection model based on canopy architecture. *IEEE Transactions on Geoscience and Remote Sensing*, *35*, 1316–1337.

Chen, J. M., & Leblanc, S. G. (2001). Multiple scattering scheme useful for geometric optical modelling. *IEEE Transactions on Geoscience and Remote Sensing*, *39*, 1061–1071.

Chen, J. M., Pavlic, G., Brown, L., Cihlar, J., Leblanc, S. G., White, H. P., et al. (2002). Derivation and validation of Canada-wide coarse-resolution lead area index using high-resolution satellite imagery and ground measurements. *Remote Sensing of Environment*, *80*, 165–184.

Chen, J. M., Rich, P. M., Gower, S. T., Norman, J. M., & Plummer, S. (1997). Leaf area index of boreal forests: Theory, techniques, and measurements. *Journal of Geophysical Research*, *102*(D24), 29429–29443.

Cohen, W. B., Maiersperger, T. K., Gower, S. T., & Turner, D. P. (2003). An improved strategy for regression of biophysical variables and Landsat ETM + data. *Remote Sensing of Environment*, *84*, 561–571.

Deering, D. W., (1978). Rangeland reflectance characteristics measured by aircraft and spacecraft sensors. PhD dissertation, Texas, A & M University, College Station, TX, 338 pp.

Dennison, P. E., Charoensiri, K., Roberts, D. A., Peterson, S. H., & Green, R. O. (2006). Wildfire temperature and land cover modeling using hyperspectral data. *Remote Sensing of Environment*, *100*, 212–222.

Dennison, P. E., & Roberts, D. A. (2003). Endmember selection for multiple endmember spectral mixture analysis using endmember average RMSE. *Remote Sensing of Environment*, *87*, 123–135.

Dennison, P. E., & Roberts, D. A. (2003). The effects of vegetation phenology on endmember selection and species mapping in Southern California Chaparral. *Remote Sensing of Environment*, *87*, 295–309.

Eklundh, L., Hall, K., Eriksson, H., Ardö, J., & Pilesjö, P. (2003). Investigating the use of Landsat thematic mapper data for estimation of forest leaf area index in southern Sweden. *Canadian Journal of Remote Sensing*, *29*, 349–362.

ENVI (2004). *Environment for visualizing images. Image analysis software manual (CD).* Boulder, Colorado, USA: Research Systems.

Frolking, S., Roulet, N. T., Moore, T. R., Lafluer, P. M., Bubier, J. L., & Crill, P. M. (2002). Modeling seasonal to annual carbon balance of Mer Bleue bog, Ontario, Canada. *Global Biogeochemical Cycles*, *16*, doi:10.1029/2001GB001457.

Gorham, E. (1991). Northern peatlands: Role in the carbon-cycle and probable responses to climatic warming. *Ecological Applications*, *1*, 182–195.

Gower, S. T., & Richards, J. H. (1990). Larches: Deciduous conifers in an evergreen world. *BioScience*, *40*, 818–826.

Green, A. A., Berman, M., Switzer, P., & Craig, M. D. (1988). A transformation for ordering multispectral data in terms of image quality with implications for noise removal. *IEEE Transactions on Geoscience and Remote Sensing*, *26*, 65–74.

Hall, R. J., Davidson, D. P., & Peddle, D. R. (2003). Ground and remote sensing of leaf area index Rocky Mountain forest stands, Kananaskis, Alberta. *Canadian Journal of Remote Sensing*, *29*, 411–427.

Hall, F. G., Shimabukuro, Y. E., & Huemmerich, K. F. (1995). Remote sensing of forest biophysical structure using mixture decomposition and geometric reflectance models. *Ecological Applications*, *5*, 993–1013.

Harris, A., Bryant, R. G., & Baird, A. J. (2005). Detecting near-surface moisture stress in *Sphagnum* spp. *Remote Sensing of Environment*, *97*, 371–381.

Harris, A., Bryant, R. G., & Baird, A. J. (2006). Mapping the effects of water stress on *Sphagnum*: Preliminary observations using airborne remote sensing. *Remote Sensing of Environment*, *100*, 363–378.

Heinz, D. C., & Chang, C. -I. (2001). Fully constrained least square linear spectral mixture analysis method for material quantification in hyperspectral imagery. *IEEE Transactions on Geoscience and Remote Sensing*, *39*, 529–545.

Hu, B., Miller, J. R., Chen, J. M., & Hollinger, A. (2004). Retrieval of canopy leaf area index in the BOREAS flux tower sites using linear spectral mixture analysis. *Remote Sensing of Environment*, *89*, 176–188.

Isaaks, E. H., & Srivastava, R. M. (1989). *An introduction to applied geostatistics.* New York, USA: Oxford University Press.

Johnson, J. R., Staid, M. L., Titus, T. N., & Becker, K. (2006). Shocked plagioclase signatures in Thermal Emission Spectrometer data of Mars. *Icarus*, *180*, 60–74.

Jordan, C. F. (1969). Derivation of leaf area index from quality of light on the forest floor. *Ecology*, *50*, 663–666.

Kucharik, C. J., Norman, J. M., & Gower, S. T. (1998). Measurements of branch area and adjusting leaf area index indirect measurements. *Agricultural and Forest Meteorology*, *91*, 69–88.

Kruse, F. A., Lefkoff, A. B., Boardman, J. W., Heidebrecht, K. B., Shapiro, A. T., Barloon, J. P., et al. (1993). The Spectral Image-Processing System (Sips) — interactive visualization and analysis of imaging spectrometer data. *Remote Sensing of Environment*, *44*, 145–163.

Lafleur, P. M., Hember, R. A., Admiral, S. W., & Roulet, N. T. (2005). Annual and seasonal variability in evapotranspiration and water table at a shrub-covered. *Hydrological Processes*, *19*, 3533–3550.

Li, L., & Mustard, J. F. (2003). Highland contamination in lunar mare soils: Improved mapping with multiple end-member spectral mixture analysis. *Journal of Geophysical Research*, *108*(E6), doi:10.1029/2002JE001917.5033.

Liu, J., Chen, J. M., Cihlar, J., & Park, W. M. (1997). A process-based boreal ecosystem productivity simulator using remote sensing inputs. *Remote Sensing of Environment*, *62*, 158–175.

Moore, T. R., Bubier, J. L., Frolking, S. E., Lafleur, P. M., & Roulet, N. T. (2002). Plant biomass and production and CO_2 exchange in an ombrotrophic bog. *Journal of Ecology*, *90*, 25−36.

Moore, T. R., Roulet, N. T., & Waddington, J. M. (1998). Uncertainty in predicting the effect of climatic change on the carbon cycling of Canadian peatlands. *Climatic Change*, *40*, 229−245.

Norman, J., & Welles, J. (1991). Instruments for indirect measurements of canopy architecture. *Agronomy Journal*, *82*, 818−825.

Okin, G. S., Roberts, D. A., Murray, B., & Okin, W. J. (2001). Practical limits on hyperspectral vegetation discrimination in arid and semiarid environments. *Remote Sensing of Environment*, *77*, 212−225.

Olaczek, R. (1986). Outline of larch ecology and phytocenology. In S. Bialobok (Ed.), *Larch (Larix Mill.)* (pp. 381−440). Warsaw, Poland: PWN-Publishers.

Payette, S., & Rochefort, L. (2001). *Écologie des tourbières du Québec-Labrador. Les Presses de l'Université Laval, Sainte-Foy, Canada.* .

Painter, T. H., Dozier, J., Roberts, D. A., Davis, R. E., & Green, R. O. (2003). Retrieval of subpixel snow-covered area and grain size from imaging spectrometer data. *Remote Sensing of Environment*, *85*, 64−77.

Peddle, D. R., Hall, F. G., & LeDrew, E. F. (1999). Spectral mixture analysis and geometric-optical reflectance modeling of boreal forest biophysical structure. *Remote Sensing of Environment*, *67*, 288−297.

Petrou, M., & Foschi, P. G. (1999). Confidence in linear spectral unmixing of single pixels. *IEEE Transactions on Geoscience and Remote Sensing*, *37*, 624−626.

Rashed, T., Weeks, J. R., Roberts, D. A., Rogan, J., & Powell, R. (2003). Measuring the physical composition of urban morphology using multiple endmember spectral mixture models. *Photogrammetric Engineering and Remote Sensing*, *69*, 1011−1020.

Roberts, D. A., Dennison, P. E., Gardner, M., Hetzel, Y., Ustin, S. L., & Lee, C. (2003). Evaluation of the potential of Hyperion for fire danger assessment by comparison to the Airborne Visible/Infrared Imaging Spectrometer. *IEEE Transactions on Geoscience and Remote Sensing*, *41*, 1297−1310.

Roberts, D. A., Gardner, M., Church, R., Ustin, S., Scheer, G., & Green, R. O. (1998). Mapping Chaparral in the Sierra Monica Mountains using multiple endmember spectral mixture models. *Remote Sensing of Environment*, *65*, 267−279.

Roberts, D. A., Smith, M. O., & Adams, J. B. (1993). Green vegetation, nonphotosynthetic vegetation, and soils in AVIRIS data. *Remote Sensing of Environment*, *44*, 255−269.

Roberts, D. A., Ustin, S. L., Ogunjemiyo, S., Greenberg, J., Dobrowski, S. Z., Chen, J., et al. (2004). Spectral and structural measures of northwest forest vegetation at leaf to landscape scales. *Ecosystems*, *7*, 545−562.

Roulet, N. T., Lafleur, P., Richard, P. J. H., Moore, T. R., Humphreys, E., & Bubier, J. (2006). Contemporary carbon balance and late Holocene carbon accumulation in a northern peatland. *Global Change Biology*, *12*, 1−15, doi:10.1111/j.1365-2486.2006.01292.x.

Schweik, C. M., & Green, G. M. (1999). The use of spectral mixture analysis to study human incentives, action, and environmental outcomes. *Social Science Computer Review*, *17*, 40−63.

Song, T. (2005). Spectral mixture analysis for subpixel vegetation fractions in the urban environment: How to incorporate endmember variability? *Remote Sensing of Environment*, *95*, 248−263.

Sonnentag, O., Talbot, J., Chen, J. M., & Roulet, N. T. (in press). Using direct and indirect measurements of leaf area index to characterize the shrub canopy in an ombrotrophic peatland. *Agricultural and Forest Meteorology.*

Tarnocai, C., Kettles, I. M., & Lacelle, B., (2000). *Peatlands of Canada Map.* Geological Survey of Canada, Open File 3834. Scale 1: 6 500 000. Natural Resources Canada, Ottawa.

Tompkins, S., Mustard, J. F., Pieters, C. M., & Forsytth, D. W. (1997). Optimization of endmembers for spectral mixture analysis. *Remote Sensing of Environment*, *59*, 472−489.

Theseira, M. A., Thomas, G., Taylor, J. C., Gemmell, F., & Varjo, J. (2003). Sensitivity of mixture modelling to end-member selection. *International Journal of Remote Sensing*, *24*, 1559−1575.

Turunen, J., Tomppo, E., Tolonen, K., & Reinikainen, A. (2002). Estimating carbon accumulation rates of undrained mires in Finland — application to boreal and subarctic regions. *Holocene*, *12*, 69−80.

Vermote, E. F., Tanré, D., Deuzé, J. L., Herman, M., & Morcrette, J. -J. (1997). Second simulation of the satellite signal in the solar spectrum, 6S: An overview. *IEEE Transactions on Geoscience and Remote Sensing*, *35*, 675−686.

Wheeler, B. D., & Proctor, M. C. F. (2000). Ecological gradients, subdivisions, and terminology of North-West European mires. *Journal of Ecology*, *88*, 187−203.

Wu, C., & Murray, A. T. (2003). Estimating impervious surface distribution by spectral mixture analysis. *Remote Sensing of Environment*, *84*, 493−505.